This section presents the framework for the seismic risk analysis and discusses the results from this analysis. The first step in evaluating the seismic risk of the Delta and Suisun levees is to assess the seismic hazard of the site. The input from seismic hazard analysis is then used for evaluating the seismic vulnerability of these levees. The effects of earthquakes may be the most significant natural hazard that can impact the Delta and the Suisun levees. These levees face increasing risk of damage and failure from a moderate to severe earthquake in the San Francisco Bay region.

The Working Group on California Earthquake Probabilities (WGCEP 2003) estimated that probability is increasing that the project region will experience a large ($M \geq 6.7$) earthquake during the 2002 to 2031 period. In 2002, the estimated probability that such an earthquake would occur during the succeeding 30 year period was 62%, and this value will increase with time. The Seismology Technical Memorandum presents more detailed information on elements of the seismic risk analysis.

6.1 EVALUATION OF SEISMIC HAZARD

6.1.1 Introduction

The seismic hazard of the project site was evaluated using a probabilistic seismic hazard analysis (PSHA), which is a standard practice in the engineering seismology/earthquake engineering community (McGuire 2004). The PSHA methodology allows for the explicit consideration of epistemic uncertainties and inclusion of the range of possible conditions in the seismic hazard model, including seismic source characterization and ground motion estimation. Uncertainties in models and parameters are incorporated into the hazard analysis through the use of logic trees.

A key assumption of the standard PSHA model is that earthquake occurrences can be modeled as a Poisson process. The occurrence of ground motions at the site in excess of a specified level is also a Poisson process, if (1) the occurrence of earthquakes is a Poisson process, and (2) the probability that any one event will result in ground motions at the site in excess of a specified level is independent of the occurrence of other events.

In a departure from standard PSHAs, which assume a time-independent Poissonian process, time-dependent hazard was calculated from the major Bay Area faults using the range of models that were considered by the WGCEP. (Note, the models considered by WGCEP [2003] do not result in a 100% time-dependent hazard) The seismic hazard is calculated at selected times over the next 200 years. In this study, the team calculated the time-independent hazard in the Delta for the purposes of comparison.

The seismic hazard analysis generates probabilities of occurrence of all plausible earthquake events (defined by their locations, magnitudes, and ground motions). These are used to develop estimates of risk (defined as the annual probability of seismically induced levee failure) at selected times over the next 200 years. The products of the PSHA include hazard-consistent site-specific acceleration response spectra at selected levee sites distributed throughout the Delta area.

The products developed in this study included:

1. The annual probabilities of occurrence at selected times over the next 200 years (e.g., 2005, 2050, etc.) of plausible earthquake events, defined by their location, magnitude, and ground motion amplitude, for all seismic sources that could impact the Delta.

2. The likelihood of multiple/simultaneous levee failures during individual scenario earthquakes (includes the correlation in ground motions that occurs during an event).

3. Time-dependent seismic hazard results for six sites in the Delta in the years of 2005, 2050, 2100, and 2200 (Figures 6-1 and 6-2). The results include: fractile hazard curves for all ground motion measures the 5th, 15th, 50th (median), 85th, and 95th percentiles, and the mean; M-D (magnitude-distance) deaggregated hazard results for all ground motion measures for 0.01, 0.001, 0.002 and 0.0004 annual probabilities of exceedance; and mean hazard curves for each seismic source for each ground motion measure. The seismic hazard results are defined for a stiff soil condition.

4. Probabilistic ground shaking hazard maps for 2% and 10% probabilities of exceedance in 50 years (2475 and 475 year return periods, respectively) for peak horizontal acceleration and 0.2 and 1.0 sec spectral accelerations (SAs), and a stiff soil site condition.

6.1.2 Seismic Hazard

In their analyses to estimate earthquake probabilities along the major faults in the San Francisco Bay Area, the WGCEP (2003) used several models including non-Poissonian models that are time-dependent, i.e., they account for the size and time of the last earthquake. In this study, the probabilities of occurrence for all significant and plausible earthquake scenarios for each seismic source at specified times over the next 200 years are required for the risk analysis, which mandates heavy reliance on the results of WGCEP (2003). For many seismic sources, insufficient information exists to estimate time-dependent probabilities of occurrence and they were treated in a Poissonian manner.

Seismic source characterization is concerned with three fundamental elements: (1) the identification location and geometry of significant sources of earthquakes; (2) the maximum size of the earthquakes associated with these sources; and (3) the rate at which they occur. In this study, the dates of past earthquakes on specific faults are also required in addition to the frequency of occurrence. The source parameters for the significant faults in the site region (Figure 6-1) are characterized for input into the hazard analyses. Both areal source zones and Gaussian smoothing of the historical seismicity are used in the PSHA to account for the hazard from background earthquakes.

The fundamental seismic source characterization came from the work done by the USGS Working Group on Northern California Earthquake Potential (WGNCEP 1996), the USGS Working Group on California Earthquake Probabilities (WGCEP 2003) and the CGS's seismic source model used in the USGS National Hazard Maps (Cao et al. 2003). This characterization was updated and revised based on recent research. Table 6-1 describes the final seismic source model used in the time-independent PSHA calculations.

The basic inputs required for the PSHA and the risk analysis are the seismic source model and the ground motion attenuation relations or more accurately ground motion predictive equations.

Technical Memorandum 3 (Topical Area – Seismology) includes detailed descriptions of the faults in the area.

The seismic hazard calculations were made using the computer program HAZ38 developed by Norm Abrahamson. An earlier version of this program HAZ36 was validated as part of PG&E's submittal to the Nuclear Regulatory Committee and the new features resulting in HAZ38 were validated as part of ongoing URS work for the U.S. Department of Energy.

6.1.3 Seismic Source Characterization

The time-dependent hazard calculations are based on WGCEP (2003). The source characterization and the time-dependent earthquake probability models were used directly with computer codes obtained from the USGS to obtain rates of characteristic events for the seven major faults in the San Francisco Bay Area considered by WGCEP (2003): San Andreas, Hayward/Rodger's Creek, Calaveras, Concord/Green Valley, San Gregorio, Greenville, and Mt. Diablo referred to as the San Francisco Bay Region (SFBR) model faults. All other faults considered in the hazard analysis were modeled only with a time-independent probability model due to the lack of data to characterize time dependence for these faults.

The SFBR model consists of many rupture sources (i.e., a single fault segment or combination of two or more adjacent segments that produce an earthquake). For instance, the Greenville source has three rupture sources (southern segment (GS), northern segment (GN), and unsegmented (GS+GN). A rupture scenario is a combination of rupture sources that describe complete failure of the entire fault, i.e., the Greenville fault has three scenarios: GN and GS rupture independently, GN+GS, and a floating rupture along GN+GS. Fault rupture models are the weighted combinations of the fault-rupture scenarios. These weights were determined by each expert considering what would be the frequency (percentage) of each rupture scenario if the entire length of the fault failed completely 100 times. These weights are adjusted slightly to account for moment balancing. The rupture scenarios and adjusted model weights provide the long term mean rate of occurrence of each rupture source for each of the characterized faults. The WGCEP (2003) approach described above differs from the logic tree characterization used in typical time-independent hazard analyses. Rupture scenarios in the WGCEP (2003) model are treated as an aleatory variable. The experts were asked to consider the distribution of the rupture scenarios for each fault. Logic trees characterize rupture scenarios as epistemic uncertainty, with each rupture scenario given a weight representing the expert's estimation of how likely it is the actual rupture scenario. The rupture sources and their characteristics are shown in Table 6-2.

The time-dependent hazard is calculated using the range of earthquake probability models that were considered by WGCEP (2003). WGCEP (2003) considered five probability models that take into account various degrees physics, date of last rupture, recent seismicity rates, and slip in the 1906 earthquake. One of the models in the suite is the Poisson model, which yields time-independent probabilities. Therefore, the results using the WGCEP (2003) model are not 100% time-dependent. The five probability models (Poisson, Empirical, Brownian Passage Time (BPT), BPT-step, and Time-Predictable) are alternative methods for calculating earthquake probabilities. WGCEP (2003) applied weights to these five models for each of the seven major faults it considered (See Table 6-3). The five probability models and their weights along with the

source characterization were used to compute the rates of characteristic events on each rupture source, which would then be used in the hazard analysis. Rupture probabilities were calculated for 1-year exposure windows using starting dates of 2005, 2055, 2105, and 2205. The following modifications to the WGCEP (2003) inputs were made.

The program for computing the time-predictable probabilities for the San Andreas rupture scenarios was obtained from Dr. William Ellsworth, USGS. The inputs to this program were modified to change the exposure time to 1 year and to compute results for the four starting times. Figures 6-3 through 6-6 show the program output plots for each case.

The Empirical Model of Reasenberg et al. (2003) was used to obtain the scale factors to modify the long term rate. WGCEP (2003) used Reasenberg et al. (2003) models A through F and assigned weights of 0.1, 0.5, and 0.4 to the minimum, average, and maximum scale factor, respectively. Using the values for models A through D listed in the WGCEP (2003) Table 5.1 and scaling the linear models E and F from WGCEP (2003) Figure 5.6, the values listed in Table 6-4 were obtained.

The only modifications made for the Poisson, BPT and BPT-step model inputs were to change the exposure time to 1 year and to compute results for the four starting times.

6.1.4 Ground Motion Attenuation

To characterize the attenuation of ground motions in the PSHA, empirical attenuation relationships appropriate for the western U.S., particularly coastal California were used. All relationships provide the attenuation of peak ground acceleration (PGA) and response SA (5% damping).

New attenuation relations developed as part of the Next Generation of Attenuation (NGA) Project sponsored by the Pacific Earthquake Engineering Research Center Lifelines Program have been released to the public. These new attenuation relationships have a substantially better scientific basis than current relationships because they are developed through the efforts of five selected attenuation relationship developer teams working in a highly interactive process with other researchers who have: (a) developed an expanded and improved database of strong ground motion recordings and supporting information on the causative earthquakes, the source-to-site travel path characteristics, and the site and structure conditions at ground motion recording stations; (b) conducted research to provide improved understanding of the effects of various parameters and effects on ground motions that are used to constrain attenuation models; and (c) developed improved statistical methods to develop attenuation relationships including uncertainty quantification. Review of the NGA relationships indicate that, in general, ground motions particularly at short-periods (e.g., peak acceleration) are significantly reduced particularly for very large magnitudes ($\mathbf{M} \geq 7.5$) compared to current relationships.

At this time, only the relationships by Chiou and Youngs, Campbell and Bozorgnia, and Boore and Atkinson are available (see Pacific Earthquake Engineering Research's NGA web site) and these were used in the PSHA. The relationships were reviewed and weighted equally in the PSHA. Intra-event and inter-event aleatory uncertainties for each attenuation relationship are required for the risk analysis. The basin depth beneath the Delta ($Z_{2.5}$) was assumed to be 5 km based on Brocher (2005).

For the Cascadia subduction zone megathrust, the relationships by Youngs et al. (1997), Atkinson and Boore (2003), and Gregor et al. (written communication, 2007) were used with equal weights.

A geologic site condition needs to be defined where the hazard will be calculated. Often this condition has been parameterized as a generic condition such as rock or soil or more recently the average shear-wave velocity (V_S) in the top 100 feet (V_S30) of a site. In this analysis, the hazard will be defined for a stiff soil site condition characterized by an average V_S30 of 1,000 ft/sec. The fragility estimates for the levees are referenced to these ground motions. All of the NGA relationships use V_S30 as an input.

6.1.5 Individual Site Hazard Results

The results of the time-dependent PSHA of the six locations in the Delta are presented in terms of ground motion as a function of annual exceedance probability. This probability is the reciprocal of the average return period. Figures 6-7 to 6-12 show the mean, median, 5th, 15th, 85th, and 95th percentile hazard curves for PGA for 2005 at the six sites. These fractiles indicate the range of uncertainties about the mean hazard. A return period of 2,500 years has a factor of 50% difference between the 5th and 95th percentile values at the Montezuma Slough. The probabilistic PGA and 1.0 sec horizontal SA are listed in Table 6-5 for a return period of 2,500 years for the year 2005 as well as 2050, 2100, and 2200. The PGA values range from 0.30 g in Sacramento, which is the most eastern site on the edge of the Delta faults to 0.74 g at Montezuma Slough. The latter site is located adjacent to the Pittsburg-Kirby Hills fault.

The contributions of the various seismic sources to the mean PGA hazard in 2005 are shown on Figures 6-13 to 6-18. The controlling seismic source varies from site to site but the Southern Midland fault and Northern Midland zone are a major contributor to several sites within the Delta at a return period of 2,500 years. At long-period ground motions, e.g., 1.0 sec SA, the Southern Midland and the Cascadia subduction zone are contributing significantly to the hazard in 2005. The results are similar at PGA but at 1.0 sec SA, the San Andreas fault becomes a major contributor due to it approaching a 1906-type rupture.

The PGA contour maps for 100, 200, and 500-year return periods are shown on Figures 6-19 through 6-21.

6.1.6 Source, Magnitude and Distance Deaggregation

Figures 6-22 to 6-27 illustrate the contributions by events when the team deaggregated the mean PGA hazard by magnitude and distance bins in 2005. At the 2,500-year return period, the PGA hazard is from nearby events (< 20 km) in the **M** 6 to 7 range. For Sacramento and Stockton, the hazard is relatively low and more distant events are contributing. At long period, > 1.0 sec SA, the pattern is similar but the contribution from **M** ~8.0 San Andreas earthquakes is quite apparent.

6.2 LEVEE SEISMIC VULNERABILITY

This section provides an assessment of the Delta and Suisun Marsh levee vulnerabilities.

6.2.1 Seismic Failure Modes

The earthquake-induced levee deformations can result either in liquefaction-induced flow slides, inertia-induced seismic deformation in nonliquefiable case, or a combination of the two. The potential seismically induced modes of failure include: overtopping as a result of crest slumping and settlement, internal piping and erosion caused earthquake-induced differential deformations, sliding blocks and lateral spreading resulting in transverse cracking, and exacerbation of existing seepage problems due to deformations and cracking.

Unlike the flood-induced failures (conventional breaches, see Section 7), the seismically induced levee failures tend to extend for thousands of feet if not miles. The team reviewed past performances of levees/dams under seismic loading to identify potential seismically induced modes of failure. The review included:

1. During the 1995 Kobe earthquake, many levees slumped as a result of ground shaking. Figure 6-28a shows a picture of one of these slumped levees and as it can be seen from this figure the damage extends as far as the eye can see. Figure 6-28b shows the schematic interpretation of the damage resulting from liquefaction-induced failure.

2. During the 1940 Imperial Valley Earthquake, the irrigation canal levees experienced extensive and consistent slumping as far as the eye can see as shown on Figure 6-29. As shown by a mark in the post in the picture, the levee crest is about 7 feet high prior to the earthquake. Most of the height of the levee was slumped by liquefaction-induced flow slide failure.

3. During the 1989 Loma Prieta earthquake, levees in Moss Landing breached as a result of liquefaction-induced slumping and lateral spreading as shown on Figure 6-30.

4. During the 1971 San Fernando earthquake, Van Norman Dam experienced extensive damage. Figure 6-31 shows that the upstream portion of the dam slumped as a result of liquefaction.

Most of these historic observations show that, the earthquake-induced deformations result in both horizontal and vertical deformation. Depending on magnitude of these deformations, a levee can fail (i.e., breach or overtopping) or experience damage. The damaged levees can fail over time, especially during high runoff in the next wet season, if they are not repaired. To estimate the cost associated with repairing a damaged levee after an earthquake, a typical slumped levee cross section was first developed based on review of the patterns of slumped levees. Figure 6-32 shows a schematic of a slumped levee. The levee crest slumped more than 10 feet vertically as a result of seismically induced deformations. The emergency repair consists of raising the levee, removing portion of the slumped levee materials on the landside, and reconstructing the levee. Figure 6-32 shows the proposed emergency repair, which includes rocking the waterside slope (3:1 slope), reconstructing the levee crest, and landside slope. The berm on the landside will be constructed at much flatter slope (6:1) than the original levee (i.e., pre-earthquake levee).

6.2.2 Analysis Approach

To evaluate the levee seismic vulnerability, it is important to estimate the potential earthquake-induced deformations. The earthquake-induced levee deformations were estimated using two approaches.

The first approach consisted of performing the dynamic response of the levee and foundation to the earthquake motions (using the computer program QUAD4M), performing pseudo-static analyses to calculate yield accelerations of potential sliding blocks within the levee (using the computer program UTEXAS 3), and performing Newmark type analysis to estimate earthquake-induced deformations by combining the results from the dynamic site response and pseudo-static analyses.

The second approach, referred to as the coupled approach, the levee and foundation dynamic response and earthquake-induced deformations are calculated in a single analysis. The analytical procedure is based on nonlinear models capable of tracking the accumulation of deformations in the levee with time during the earthquake. Because the program FLAC used to analysis for nonlinear response has the capability to represent the coupled pore pressure generation during the seismic shaking, it was used to calculate directly the total deformation and slumping induced by the earthquake events in both liquefiable and nonliquefiable conditions

The deformation analyses were performed for both liquefied and nonliquefied cases. Nonliquefied cases were performed using the first approach. A limited number of verification runs were performed using the second approach to compare the earthquake-induced deformation results from both approaches.

In cases of liquefied site, two conditions were considered: liquefaction of foundation materials and liquefaction of levee fill. For levees with potentially liquefiable foundation layer, a time domain fully coupled analysis was performed using the computer program FLAC. When the levee fill or when both the levee fill and foundation materials are susceptible to liquefaction the earthquake-induced deformations tend to be very large and may cause the computer program not converge. To mitigate these conditions, a simplified use of the FLAC model was considered to capture the “post-liquefaction static slumping.” In this simplified method, the levee fill was first modeled using the pre-liquefied shear strength values, then in a quasi-static fashion, these strength values were reduced in a step-wise function to the post-liquefactions residual shear strength values. The deformations obtained by this approach would then be combined with the inertia-induced deformations from the QUAD4M-Ky-Newmark results to form the total levee-foundation deformation.

The schematic illustration of the levee and foundation (80 feet) used in the model to represent the site response, the deconvolution and propagation of the motion into the 2-D finite element model is shown on Figure 6-33.

6.2.3 Liquefaction Potential Evaluation

The potential for levee liquefaction was estimated using available borings and cone penetrometer test (CPT) data. The Levee Vulnerability team believes that levees that have granular materials with $(N1)_{60\text{-}cs}$ less than 15 would liquefy at a PGA of 0.05 g. Those observation were confirmed by the liquefaction triggering analyses where the cyclic stress demands (seismic demand) were compared to the cyclic stress resistance (soil resistance as a function of its $(N1)_{60\text{-}cs}$) as shown in

the "Levee Vulnerability Technical Memorandum." (N1)60-CS values for both levee fill and foundation sand were calculated using available borings and cone penetrometer tests (CPT) data.

CPT data obtained within the top 20 feet through the levee were digitized and converted to (N1)60-cs using the procedure proposed by Boulanger and Idriss (2004). A total of 69 (N1)60-cs values (converted from CPT data) are available, out of which 52 of them were less than 15 and rest (i.e., 17) were greater than 15. For the case of boring data, only blowcount data obtained using either a SPT or a modified California drive samplers were considered. A total of 905 (N1)60-cs values were available, out of which 657 of them were less than 15 and the rest (i.e., 248) were greater than 15. The ratio of (N1)60-cs less than 15 to the numbers for SPT borings and CPT soundings (converted values) are about 72% and 75%, respectively. The liquefaction potential analysis for both levee fill and foundation sand are described in the Levee Vulnerability Technical Memorandum.

6.2.4 Vulnerability Classes

The system of levees in the Delta study area was divided into vulnerability classes using factors that differentiate the performance of the levees when subjected to the same seismic event. The definition of the vulnerability classes was based on available subsurface information, levee fill conditions and geometry, past performance, and maintenance history. This information was used to develop a GIS-based Delta levee catalogue providing data regarding the spatial and temporal variation in the levee and foundation conditions. This catalogue was then used to develop typical cross-sections based on an idealized geometry and subsurface materials.

The geo-database was integrated into the GIS system for creating and displaying several maps such as the peat/organic soil thickness map. Following are the GIS maps used to define the vulnerability classes under seismic loading:

1. Organic Thickness map (Figure 6-34)
2. (N1)60-cs for Foundation Sand (Figure 6-35)
3. N1)60-cs for Levee Sand (Figure 6-36)

The following factors were considered in defining levee vulnerability classes for seismic analyses:

- Levee material type (clay levees, and sand levees with potential for liquefaction)
- Thickness of peat and organics (0, 0.1-10.0 ft, 10.1-20.0 ft, and > 20 ft)
- Liquefaction potential of foundation sand ((N1)60-cs of 0-5, 5.1-10, 10.1-20, and >20
- Levee geometry (steep waterside slope, and non-steep water side slope)

The vulnerability classes for Delta were developed considering only possible combinations of above factors that would differentiate the seismic behavior of levees for the geographic region. For example, if a levee reach had liquefiable levee material with (N1)60-cs < 20, the seismic behavior of that levee reach would not be controlled by both the liquefaction potential of the foundation sand and levee geometry. The variations in peat properties (friction angle (f) and cohesion (c)), peat thickness, and corrected clean sand equivalent SPT blow count ((N1)60-cs) were treated as random variables, where applicable (see Table 6-5a). For example, vulnerability class 6 has (N1)60-cs of the foundation sand and peat thickness as random input variables; the

variations in peat properties are not applicable for this class because it has relatively minimal influence on seismic behavior compared to the influence of (N1)60-cs of the foundation sand. Conversely, vulnerability class 15 has the soil properties (c, f) as random input variables; (N1)60-cs of the foundation sand and peat thickness are not applicable for this class because of their minimal influence on seismic behavior. Table 6-5a lists the vulnerability classes considered for seismic analyses for Delta along with the random variables considered for each vulnerability class.

The levees in Suisun Marsh were divided into two vulnerability classes mainly based on liquefaction potential of levee and foundation sand. Table 6-5a also lists the vulnerability classes considered for Suisun Marsh along with the details of random variables.

For each vulnerability class, the earthquake-induced permanent deformation from the various earthquake events was estimated using the logic tree approach presented in Figure 6-37. The logic tree approach requires identifying the material properties that should be treated as random variables and characterized in terms of their probability distributions. Several potential material properties were considered and the sensitivity of the estimated deformations to the variations in each property was assessed. The material properties whose variations showed relatively little effect on deformation were considered to be deterministic in the probabilistic analysis and best point estimates of these properties were used in the calculation of deformation for different vulnerability classes. The material properties whose variations showed a significant effect on deformation were considered to be random variables and their probability distributions were defined based on a statistical analysis of available data. These probability distributions quantify the aleatory uncertainty in the materials properties.

A lognormal distribution was assumed for each random input variable because it is a commonly accepted probability distribution of soil properties and the shape of this distribution provides a reasonable fit to the distribution of field data. A lognormal distribution is completely defined by two statistical parameters - the median and the logarithmic standard deviation.

The following section describes the selection of material properties that were defined to be random variables, and the estimation of the statistical parameters that define their probability distributions.

Selection of Random Variables and Estimation of Their Statistical Distribution

1) Non Liquefiable case

For the non-liquefiable case, the following variables were considered in the sensitivity analysis:

- Strength parameters of peat
- Variation of water side slope
- Variation of land side slope
- Variation of water level elevation
- Variation of G/Gmax and Damping curves of peat

Variation in the land side slope assumed to have insignificant effects on the calculations seismic deformations, since deep sliding surfaces through peat controls the seismic deformations. The

variation of water level elevation of the slough also will not have much impact on calculations seismic deformations, since island side sliding surfaces controls the deformations.

The effect of variation of G/Gmax and Damping curves of PEAT were considered using the set of curves provided by Wehling (2001) for uncertainty in their estimation. It was found out from these analyses that the variation of G/Gmax and Damping curves of PEAT has almost no effect on the calculated deformations.

The variation of strength parameters of peat will have some impact on calculation of seismic deformations. Therefore, the available p-q data of peat were utilized to calculate the standard deviations in cohesion and friction of peat. Results are shown in Figures 6-2 and 6-3. These standard deviations were applied to the calibrated strength parameters of peat.

The steep waterside slopes are expected to yield large displacements during seismic event. We have performed sensitivity analyses assuming steep waterside slope of 1.5:1, for all the idealized cross sections considered.

2) Liquefiable Case

For the liquefiable cases deformation is mainly controlled by the residual strength of the liquefiable sand layer. Since, we have used the correlation with (N1)60-CS to estimate residual strength of liquefiable sand layer, variation in (N1)60-CS value was used to estimate the standard deviation of residual strength values. Sensitivity analyses were performed for variation in residual strength values of the liquefiable foundation layer and liquefiable embankment fill..

6.2.5 Results of Seismic Vulnerability Analysis

Each vulnerability class of levee and foundation is characterized by a set of random variables and their statistical distributions. Based on statistical analysis of available data and published information, probability distribution functions of the input variables that exhibit random spatial variability were developed. Monte Carlo simulations were used to generate values of the input random variables. The seismic response of each vulnerability class (idealized cross section) was estimated for the range of earthquake magnitudes and reference site PGAs. The following are few illustrative example form the seismic response analysis. The results of all levee vulnerability classes can be found in the "Levee Vulnerability Technical Memorandum."

1. Calculated Newmark Displacements for Nonliquefiable Section with 15 feet of Peat (Figure 6-38)

2. Calculated FLAC Displacements for Section with Liquefiable Foundation and 15 feet of Peat (Figure 6-39)

3. Displacements for Section with Liquefiable Levee and 15 feet of Peat (Figure 6-40)

Multiple regression equations were developed (mean value and distribution around the mean) to represent the seismically induced deformation as a function of earthquake magnitude and reference site PGA's for various confidence levels (called levee "response" curves).

To estimate the probability of levee failure under a seismic loading, the response curves need to be combined with a "fragility" curve that represents the probability of failure given a magnitude and associated PGA.

It was agreed with the Technical Advisory Committee that probability of failure during seismic event should be correlated to both the calculated vertical deformation and initial free board. For simplicity, probability of failure was correlated to a ratio between vertical deformation and initial free board. Expert elicitation was sought to provide input for this correlation. Using this input from the experts, three curves corresponding to the probabilities of 16%, 50%, and 84% were developed relating the probability of failure to the relative loss of freeboard (i.e., ratio of vertical deformation/initial freeboard). Figure 6-41 shows the three curves. These curves define the epistemic uncertainty in the seismic fragility curve. More detail on the levee vulnerability approach can be found in the Levee Fragility Technical Memorandum.

The product of the two sets of functions (response and fragility curves) resulted in the estimation of the levee probability of failure as a function of the seismic loading, Figure 6-42. Examples of product output from the levee seismic vulnerability task are shown on Figure 6-43 and in Table 6-6. Table 6-6 is only samples of a much larger data set that constitute the input into the risk model. The data are used in the risk model and combined with the probability of occurrence of the various stressing events to produce the expected probability of failures of the Delta and Suisun Marsh levees.

6.3 SEISMIC SYSTEM MODEL

6.3.1 Spatial Modeling of Physical Response of Levees to Seismic Events

Section 6.2 described the geotechnical model used to assess seismic deformation of individual levees in different vulnerability classes subjected to a given earthquake and the probability model to assess the probability of a breach of a levee reach given the estimated seismic deformation. To assess the risk of simultaneous, multiple levee failures under a given earthquake, the team also need to model the simultaneous physical behavior of all levees in the study area subjected to the ground motions from a specified earthquake. Such a model needs to account for the spatial continuity of levees and define how levees within and across contiguous spatial zones are likely to behave in a given earthquake. This model of physical behavior should be based on empirical evidence and knowledge of soils behavior during earthquakes.

This section first provides an overview of the spatial physical model of representing levees and foundations around different islands and describes the key assumptions made in modeling the spatial behavior during an earthquake. Next, the model to estimate the probability of simultaneous multiple breaches is presented.

6.3.2 Spatial Model of Representing Levees around Different Islands

Observations of levee performance during previous earthquakes and an understanding of soils behavior during seismic ground motions suggest that levee sections within contiguous spatial zones of similar geotechnical properties behave differently from those across such contiguous zones. These differences and the corresponding modeling assumptions are described below.

Levee sections within a contiguous spatial zone around a given island with similar geotechnical properties are generally observed to behave as a single structural unit when subjected to a given earthquake. Empirical evidence suggests that, if the earthquake motions are strong enough, long stretches of contiguous levees spanning several miles are likely to slump substantially. An actual

through levee breach may occur at some random location within this span of slumped levees among the contiguous zone of levees. As a breach develops at a particular location, the stress on other levee sections within the same contiguous zone may dissipate making it less likely that a simultaneous breach at another location within the same contiguous spatial zone would develop. For this analysis, the team assumed that only one breach could occur within each contiguous spatial and the probability of more than one simultaneous breaches within a given contiguous spatial zone is negligible.

Levee sections across different contiguous spatial zones generally behave independently of each other. Thus, the occurrence of a breach within one contiguous spatial zone would not preclude the possibility of another simultaneous breach in some other contiguous spatial zone. Furthermore, a breach within a given contiguous spatial zone during a specified earthquake would not alter the likelihood of a breach in a different contiguous spatial zone (either on the same or different island).

Using this concept of contiguous spatial zones and the likely difference in the levee performance within and across different spatial zones, the team developed a spatial model of simultaneous levee response across the entire study area under a given earthquake.

The scale of resolution in estimating such geotechnical properties as peat thickness, levee crest elevations, and soil blow counts, based on available data, was of the order of 1,000 feet. Therefore, levees around each analysis zone (i.e., island) were divided into 1,000-foot individual reaches. Each levee reach was assigned to one and only vulnerability class using the geotechnical variables that were relevant to assessing the levee response to an earthquake. Contiguous spatial zones around each island were defined by identifying contiguous levee reaches that belonged to the same vulnerability class.

Consider, for example, an island with a levee perimeter of 50 individual 1,000-foot reaches. Furthermore, 20 contiguous reaches belong to Vulnerability Class A, while the remaining 30 contiguous reaches belong to Vulnerability Class B. For this island, two contiguous spatial zones would be defined, one comprising the first 20 reaches and the other comprising the remaining 30 reaches. Note that we define a contiguous spatial zone based on physically connected levee reaches. Therefore, levees around another island even when they belong to the same vulnerability class would not be considered to be contiguous to those on the first island and hence would belong to a different contiguous spatial zone. Figure 6-44 shows a schematic of how contiguous spatial zones would be defined for two different islands. The same concept is used to define contiguous spatial zones over the entire study area.

6.3.3 Model for Estimating Probability of Simultaneous Levee Failures

An objective is to assess the probability of simultaneous levee failures in the study area when subjected to a specified earthquake that imposes different ground motions to different levee reaches. Assume that the study area has been divided into contiguous spatial zones using the approach described on Figure 6-44. Let Z_{ij} denote the j-th contiguous spatial zone around the i-th island and R_{ijk} denote the k-th levee reach within the j-th contiguous spatial zone around the i-th island.

6.3.4 Probability of One Breach within a Given Contiguous Spatial Zone

Let m denote the magnitude of a specified earthquake event and **a**(m) denote the spatial field of the ground motions over the study area resulting from this event. The spatial field **a**(m) comprises (a_{ijk}|m), which is the ground motion experienced at the levee reach R_{ijk} from the specified earthquake for all i, j, and k. Using the levee fragility model described in Section 6.3.3, we can calculate the probability of a breach of the reach R_{ijk} when subjected to the ground motion (a_{ijk}|m). Let PF(R_{ijk}|a_{ijk}, m, fb_{ijk}) denote the probability of a breach of the reach R_{ijk} when subjected to a ground motion of a_{ijk} from an earthquake of magnitude m; and the initial freeboard is fb_{ijk}. The freeboard is calculated as the difference between the levee crest elevation and the mean daily higher high water level.

The team assumed that only one breach is possible within a given contiguous spatial zone. Let PF(Z_{ij}|m, **a**(m)) denote the probability of a breach for the contiguous spatial zone Z_{ij} given the earthquake magnitude m and the ground motion field **a**(m). This probability will be assumed to be equal to the maximum probability of a breach for each of the reaches within the contiguous spatial zone; that is,

$$PF(Z_{ij}|m, \mathbf{a}(m)) = \text{maximum}(PF(R_{ijk}|m, a_{ijk,} fb_{ijk}) \text{ over all k.} \quad (1)$$

6.3.5 Probability of Simultaneous Multiple Breaches over All Contiguous Spatial Zones

The probability of a breach in a given contiguous zone will be assumed to be independent of the probability of a breach in any other contiguous spatial zone. Therefore, the joint probability of simultaneous breaches over specified contiguous spatial zones will be calculated as the product of the probability of a breach for each of those contiguous spatial zones and the probability of no breach on all other contiguous spatial zones. Figure 6-45 shows the logic tree that could be used to calculate the probabilities of different number of breaches over different contiguous spatial zones over all islands within the study area.

Consider, for example, two islands – A and B, with 2 and 3 contiguous spatial zones, respectively. As an illustration of the joint probability calculation, the probability of two breaches on Island A, but no breaches on Island B can be obtained from:

P(two breaches on Island A and 0 breaches on Island B) =

$$PF(Z_{A1}|m, \mathbf{a}(m)) \times PF(Z_{A2}|m,\mathbf{a}(m)) \times (1-PF(Z_{B1}|m, \mathbf{a}(m)) \times (1- PF(Z_{B2}|m, \mathbf{a}(m)) \times (1- PF(Z_{B3}|m, \mathbf{a}(m)) \quad (2)$$

The probability of a breach in any given contiguous zone is found from Equation 1.

6.3.6 Probability of Damaged Levees

As stated above, when levees are damaged during an earthquake, the extent of damage spans a long distance, typically several miles. Based on this observation, the team assumed that if damage were to occur in a given contiguous spatial zone, the entire length of that zone would experience slumping and significant damage. One could derive the probability of damage by making certain assumptions consistent with empirical observations. The team assumed that n independent contiguous spatial zones exist and the mean rate of breached zones is m/n. That is, m out of n zones would be expected to experience a breach during a specified earthquake.

Empirical observations suggest that a breach is likely to be accompanied by 5 to 10 miles of slumped/damaged levees. Assuming a mid-point of 8 miles of damaged levees per breach and a typical length of 4 miles for a contiguous spatial zone, two zones, on the average, would be damaged per breach. Therefore, the mean rate of damaged levee zones would be of the order of 2m/n. Thus, for example, if one zone is breached, two zones of 4 miles each (a total of 8 levee miles), on the average, would be damaged, suggesting that the probability of significant damage to a given contiguous zone is twice the probability of a breach in the zone. If a zone were to breach, it would also experience significant damage. That is, given that a zone breaches, the probability of damage on that zone would be one.

Table 6-1 Bay Area Time-Independent Seismic Source Parameters

Fault Name	Probability of Activity[1]	Rupture Scenario[2]	Segment Name	Rupture Length[3]	Width[4]	Dip[5]	Direction of Dip[6]	Sense of Slip[7]	Magnitude[8]	Slip Rate[9]	Notes
San Andreas (Northern and Central)	1.0	Unsegmented (0.5)	1906	473	13 ± 3	90	N/A	SS	7.9	24 ± 3	Characterization based on WGCEP (2003). Unsegmented rupture scenario is a repeat of the 1906 **M** 7.9 San Francisco earthquake.
		Two Segments (0.2)	Offshore + North Coast	326	11 ± 2	90	N/A	SS	7.7	24 ± 3	
			Peninsula + Santa Cruz Mountains	147	13 ± 2	90	N/A	SS	7.4	17 ± 4	
		Three Segments (0.1)	Offshore + North Coast	326	11 ± 2	90	N/A	SS	7.7	24 ± 3	
			Peninsula	85	13 ± 2	90	N/A	SS	7.2	17 ± 4	
			Santa Cruz Mountains	62	15 ± 2	90	N/A	SS	7.0	17 ± 4	
		Floating Earthquake (0.2)	N/A	N/A	13 ± 3	90	N/A	SS	6.9	24 ± 3	
Calaveras	1.0	Unsegmented (0.05)	Northern + Central + Southern Calaveras	123	11 ± 2	90	N/A	SS	6.9	4 (0.2) 6 (0.4) 15 (0.3) 20 (0.1)	Characterization of WGCEP (2003) modified by recent paleoseismic data of Kelson (written communication, 2006).
		Two Segments (0.05)	Northern Calaveras	45	13 ± 2	90	N/A	SS	6.8	6 ± 2	
			South + Central Calaveras	78	11 ± 2	90	N/A	SS	6.4	15 ± 3	
		Three Segments (0.3)	Northern Calaveras	45	13 ± 2	90	N/A	SS	6.8	6 ± 2	
			Central Calaveras	59	11 ± 2	90	N/A	SS	6.2	15 ± 3	
			Southern Calaveras	19	11 ± 2	90	N/A	SS	5.8	15 ± 3	
		Segment + Floating Earthquake (0.5)	Northern Calaveras	45	13 ± 2	90	N/A	SS	6.8	6 ± 2	
			Floating Earthquake on Central + South Calaveras	N/A	11 ± 2	90	N/A	SS	6.2	15 ± 3	
		Floating Earthquake (0.1)	N/A	N/A	11 ± 2	90	N/A	SS	6.2	4 (0.2) 6 (0.4) 15 (0.3) 20 (0.1)	
Concord – Green Valley	1.0	Unsegmented (0.35)	N/A	56	14 ± 2	90	N/A	SS	6.7	5 ± 3	Characterization based on WGCEP (2003).
		Three Segments (0.1)	Concord	20	16 ± 2	90	N/A	SS	6.25	4 ± 2	
			Southern Green Valley	22	14 ± 2	90	N/A	SS	6.25	5 ± 3	
			Northern Green Valley	14	14 ± 2	90	N/A	SS	6.0	5 ± 3	
		Two Segments (0.15)	Concord	20	16 ± 2	90	N/A	SS	6.25	4 ± 2	
			Green Valley	36	14 ± 2	90	N/A	SS	6.5	5 ± 3	
		Two Segments (0.15)	Concord + Southern Green Valley	42	14 ± 2	90	N/A	SS	6.6	5 ± 3	
			Northern Green Valley	14	14 ± 2	90	N/A	SS	6.0	5 ± 3	
		Floating Earthquake (0.25)	N/A	N/A	14 ± 2	90	N/A	SS	6.2	5 ± 3	
Greenville	1.0	Unsegmented (0.4)	N/A	58	15 ± 3	90	N/A	SS	6.9	2 (0.2) 4 (0.6) 6 (0.2)	Characterization based on paleoseismic data from Sawyer and Unruh (2002). and T.L. Sawyer (personal communication, 2006).
		Floating (0.6)	N/A	N/A	15 ± 3	90	N/A	SS	6.5	2 (0.2) 4 (0.6) 6 (0.2)	

Table 6-1 Bay Area Time-Independent Seismic Source Parameters

Fault Name	Probability of Activity[1]	Rupture Scenario[2]	Segment Name	Rupture Length[3]	Width[4]	Dip[5]	Direction of Dip[6]	Sense of Slip[7]	Magnitude[8]	Slip Rate[9]	Notes
Hayward – Rodgers Creek	1.0	Unsegmented (0.05)	Hayward + Rodgers Creek	151	12 ± 2	90	N/A	SS	7.3	9 ± 2	Characterization based on WGCEP (2003) model.
		Two Segment (A) (0.1)	North Hayward + Rodgers Creek	98	12 ± 2	90	N/A	SS	7.1	9 ± 2	
			Southern Hayward	53	12 ± 2	90	N/A	SS	6.7	9 ± 2	
		Two Segment (B) (0.3)	Rodgers Creek	63	12 ± 2	90	N/A	SS	7.0	9 ± 2	
			Hayward	88	12 ± 2	90	N/A	SS	6.9	9 ± 2	
		Three Segment (0.5)	Rodgers Creek	63	12 ± 2	90	N/A	SS	7.0	9 ± 2	
			North Hayward	35	12 ± 2	90	N/A	SS	6.5	9 ± 2	
			Southern Hayward	53	12 ± 2	90	N/A	SS	6.7	9 ± 2	
		Floating Earthquake (0.05)	N/A	N/A	12 ± 2	90	N/A	SS	6.9	9 ± 2	
Mt Diablo	1.0	Unsegmented (0.5)	N/A	31	17 ± 2	30 (0.2) 45 (0.6) 50 (0.2)	NE	R	6.7	1 (0.2) 3 (0.6) 5 (0.2)	Characterization from Unruh (2006). Fault tip inferred to approach within 5 km (0.5) to 1 km (0.5) of the surface based on restorable cross section, and on map-scale relationships between surface faults and fold axis.
		Segmented (0.5)	Mt. Diablo North	12	17 ± 2	30 (0.2) 45 (0.6) 50 (0.2)	NE	R	6.3	1 (0.2) 3 (0.6) 5 (0.2)	North: Fault tip inferred to approach within 4 km (0.5) to 2 km (0.5) of the surface based on model in restorable cross section.
			Mt. Diablo South	19	17 ± 2	30 (0.2) 45 (0.6) 50 (0.2)	NE	R	6.6	1 (0.2) 3 (0.6) 5 (0.2)	South: Fault tip inferred to approach within 5 km (0.5) to 1 km (0.5) of the surface based on model in restorable cross section, and map-scale relationships between surface faults and fold axis.
San Gregorio	1.0	Unsegmented (0.35)	Northern + Southern San Gregorio	176	13 ± 2	90	N/A	SS	7.5	1 (01) 3 (0.4) 7 (0.4) 10 (0.1)	Characterization based on WGCEP (2003) model.
		Segmented (0.35)	Northern San Gregorio	110	13 ± 2	90	N/A	SS	7.2	7 ± 3	
			Southern San Gregorio	66	12 ± 2	90	N/A	SS	7.0	3 ± 2	
		Floating Earthquake (0.3)	N/A	N/A	13 ± 2	90	N/A	SS	6.9	1 (0.1) 3 (0.4) 7 (0.4) 10 (0.1)	
Briones (zone)	1.0	N/A	N/A	23	15 ± 3	90	N/A	SS	6.5	0.5 (0.2) 1.0 (0.6) 2.0 (0.2)	Characterization from Unruh (2006).
Collayomi	1.0	Unsegmented (1.0)	N/A	29	10	90	N/A	SS	6.5	0.6 ± 0.3	Cao et al. (2003)
Cordelia	1.0	Unsegmented (1.0)	N/A	19	15 ± 3	90	N/A	SS	6.6	0.05 (0.4) 0.6 (0.5) 1.0 (0.1)	Characterization based on paleoseismic data from Harlan Tait & Associates (1994).
CRSB North of Delta	1.0	Multisegment (0.1)	Mysterious Ridge	35	13 ± 2	25 ± 5	W	R	6.7	1.0 (0.7) 3.5 (0.3)	Characterization revised from WGNCEP (1996) using data from O'Connell et al. (2001). Fault tip of Mysterious Ridge, Trout Creek, and Gordon Valley at depths of 7, 9, and 8 km, respectively. Segment lengths have an uncertainty of ± 5 km.
			Trout Creek + Gordon Valley	38	13 ± 2	25 ± 10	W	R	6.8	0.5 (0.3) 1.25 (0.6) 2.0 (0.1)	
		Segmented (0.9)	Mysterious Ridge	35	13 ± 2	25 ± 5	W	R	6.7	1.0 (0.7) 3.5 (0.3)	
			Trout Creek	20	13 ± 2	20 ± 5	W	R	6.5	0.5 (0.3) 1.25 (0.6) 2.0 (0.1)	

Table 6-1 Bay Area Time-Independent Seismic Source Parameters

Fault Name	Probability of Activity[1]	Rupture Scenario[2]	Segment Name	Rupture Length[3]	Width[4]	Dip[5]	Direction of Dip[6]	Sense of Slip[7]	Magnitude[8]	Slip Rate[9]	Notes
CRSB North of Delta (cont'd.)			Gordon Valley	18	13 ± 2	30 ± 5	W	R	6.4	0.5 (0.3) 1.25 (0.6) 2.0 (0.1)	
Cull Canyon-Lafayette-Reliz Valley	1.0	Unsegmented (1.0)	N/A	25	12 ± 3	90°	N/A	SS	6.6	0.5 (0.2) 1.0 (0.6) 3.0 (0.2)	Characterization from Unruh and Kelson (2002) and Unruh (2006).
Foothill Thrust System	0.6	Floating Earthquake (1.0)	N/A	N/A	15 ± 3	60	SW	R	6.25 (0.3) 6.5 (0.3) 6.75 (0.3) 7.0 (0.1)	0.2 (0.2) 0.5 (0.6) 0.8 (0.2)	Simplified characterization based on WGCEP (2003) subgroup and recent studies as summarized in Kennedy et al. (2005). Incorporates Berrocal, Shannon-Monte Vista, Stanford, and Cascade faults. Although evidence of Holocene and latest Pleistocene fold deformation along this fault zone is clear (Hitchcock and Kelson 1999; Bullard et al. 2004), the fault is assigned a Probability of Activity of 0.6 to address the uncertainty as to whether the fault is an independent seismic source capable of generating moderate to large magnitude earthquakes. The seismogenic potential of the range front thrust faults is not well known. Aseismic slip (Bürgmann et al. 1994) and coseismic slip during large magnitude events on the San Andreas fault system fault, such as occurred during the 1989 Loma Prieta earthquake (Haugerud and Ellen 1990) may account for some or all of the local San Andreas fault-normal contraction, precluding the need for independent large magnitude events on the compressive structures. (Angell et al. 1997; Hitchcock and Kelson 1999).
Hunting Creek-Berryessa	1.0	Unsegmented (1.0)	N/A	60	12	90	N/A	SS	6.9	6 ± 3	Cao et al. (2003)
Las Trampas	0.5	Unsegmented	N/A	12	14 ± 3	45° 60° 75°	SW	R	6.2	0.5 (0.2) 1.0 (0.6) 3.0 (0.2)	Characterization from Unruh and Kelson (2002) and Unruh (personal communication, 2006).
Los Medanos Fold and Thrust Belt	1.0	Unsegmented (0.2)	N/A	15	17 ± 2	30 (0.2) 45 (0.2) 60 (0.6)	NE	R	6.5	0.3 (0.3) 0.5 (0.4) 0.7 (0.3)	Characterization based on Unruh and Hector (1999) and the Thrust Fault Subgroup of the 1999 Working Group. Roe thrust: fault tip inferred to lie between 0 km and 1 km depth based on analysis of gas well data.
		Segmented (0.8)	Roe Island	5	5 ± 2	30 (0.2) 45 (0.2) 60 (0.6)	NE	R	5.8	0.3 (0.3) 0.5 (0.4) 0.7 (0.3)	Roe thrust: fault tip inferred to lie between 0 km and 1 km depth based on analysis of gas well data.
			Los Medanos	10	10 ± 2	30 (0.2) 45 (0.6) 60 (0.2)	NE	R	6.0	0.3 (0.3) 0.5 (0.4) 0.7 (0.3)	Los Medanos thrust: fault tip inferred to lie between 1 km and 2 km depth based on analysis of gas well data and construction of geologic cross sections.
Maacama-Garberville	1.0	Unsegmented (1.0)	N/A	182	12	90	N/A	SS	7.4	9.0 ± 2.0	Cao et al. (2003)
Midway/ Black Butte	1.0	Floating Earthquake (1.0)	N/A	31	15 ± 3	70 ± 10	W	RO	6.25 (0.2) 6.5 (0.4) 6.75 (0.4)	0.1 (0.3) 0.5 (0.4) 1.0 (0.3)	The Black Butte fault is a documented late Quaternary-active reverse (oblique?) fault (Sowers et al. 1992) that appears to be related to the late Cenozoic dextral Midway fault by a short left-restraining bend. Limited data are available on slip rate and rupture behavior. The slip rate estimate is based on uplift of middle to early Pleistocene pediment surface across the Black Butte fault (Sowers et al. 1992) and an inferred H:V ratio for the components of slip of ≤ 3:1.
Monterey Bay-Tularcitos	1.0	Unsegmented (1.0)	N/A	84	14	90	N/A	SS	7.1	0.5 ± 0.4	Cao et al. (2003)

Table 6-1 Bay Area Time-Independent Seismic Source Parameters

Fault Name	Probability of Activity[1]	Rupture Scenario[2]	Segment Name	Rupture Length[3]	Width[4]	Dip[5]	Direction of Dip[6]	Sense of Slip[7]	Magnitude[8]	Slip Rate[9]	Notes
Montezuma Hills (zone)	0.5	Floating Earthquake (1.0)	N/A	N/A	15 ± 5	70	W	RO	6.0 (0.3) 6.25 (0.4) 6.5 (0.3)	0.05 (0.3) 0.25 (0.4) 0.5 (0.3)	The Montezuma Hills source zone is considered as a possible independent source of seismicity based on the following: 1) the topographic and structural gradient of the hills is to the northeast, which is contrary to what would be expected if the hills were being uplifted in the hanging wall of the Midland fault; 2) the topography dies out west of the subsurface trace of the Midland fault, rather than extending up to the fault; 3) the Montezuma hills are spatially associated with the Antioch and Sherman Island faults, as well as some anomalous topography near the town of Oakley south of the Sacramento River. Alternatively, the uplift of this region is secondary tectonic deformation related to movement in the hanging wall of the Midland fault or transfer of slip from the Vernalis/West Tracy faults to the Pittsburg/Kirby Hills fault zone. Preferred orientation of modeled fault planes within zone (N20°W).
Mt Oso	0.7	Unsegmented (1.0)	N/A	25	15 ± 2	30 (0.3) 45 (0.4) 60 (0.3)	NE	R	6.9	0.5 (0.2) 1.5 (0.6) 2.5 (0.2)	Inferred thrust fault occupying the contractional stepover between the Ortigalita and Greenville faults. NE-dipping rupture geometry inferred from the SW-vergence of the Mt. Oso anticline and analogy to Mt. Diablo thrust (Unruh, Lettis and Associates, personal communication, 2006). Activity based on slip transfer from the northern Ortigalita to the southern Greenville. Fault tip at 5 km depth.
Northern Midland (zone)	1.0	Floating Earthquake (1.0)	N/A	N/A	15 ± 5	70	W	RO	6.0 (0.3) 6.25 (0.4) 6.5 (0.3)	0.1 (0.3) 0.5 (0.4) 1.0 (0.3)	Preferred orientation of modeled fault planes within zone (N30°W). North of Rio Vista, published data from gas exploration indicate that the Midland fault breaks into a zone of right-stepping en echelon fault traces. Anomalous, apparently uplifted Quaternary topography that appears to be associated with the stepover regions may be related to recent movement on a system of underlying oblique reverse faults in this zone. Tips of faults are inferred by CDOG (1982) to extend above the base of the Tertiary Markley Formation to depths of about 1.5 km, and possibly shallower. Minimum fault depth not constrained by data in CDOG (1982).
Orestimba	1.0	Unsegmented (1.0)	N/A	60	Tip 1 (0.5) 3 (0.5) Base 15 ± 3	30° (0.2) 45° (0.6) 60° (0.2)	W	R	6.7	0.2 (0.2) 0.4 (0.6) 0.6 (0.2)	Characterization based on Anderson and Piety (2001). Segment of Coast Range/Sierran block boundary(CRSB) (also referred to as the Coast Range/Central Valley fault system.). Anderson and Piety (2001) assign steeper dips (20 to 30°) to the Orestimba fault than considered in the CGS source model (Cao et al. 2003). The Thrust Subgroup of the 1999 Working Group, that provided input to WGCEP (2003), suggested a range of dip between 25° (similar to the Coalinga thrust fault) and 60° (predicted by Coulomb failure criteria).The steepness of the range along these segments from between approximately 36.5°N to 38°N suggests that the dip of the underlying structures is probably at the higher end of this range. Anderson and Piety (2001) provide estimates for the uplift rate along several segments based on the elevation of uplifted early (?) to middle Pleistocene pediment surfaces and late Pleistocene fluvial terraces (Sowars et al. 1992). These uplift rates are converted into slip rates using the range of fault dips assigned to each segment.

Table 6-1 Bay Area Time-Independent Seismic Source Parameters

Fault Name	Probability of Activity[1]	Rupture Scenario[2]	Segment Name	Rupture Length[3]	Width[4]	Dip[5]	Direction of Dip[6]	Sense of Slip[7]	Magnitude[8]	Slip Rate[9]	Notes
Ortigalita	1.0	Segmented (0.3)	Northern Ortigalita	40	15 ± 3	90	N/A	SS	6.9	0.5 (0.15) (0.35) (0.35) 2.5 (0.15)	Characterization revised from Cao et al. (2003) using recent mapping and paleoseismic data from Anderson and Piety (2001) to modify the lengths and slip rates for the north and south segments of the fault. They estimate a slip rate of 1.0-2.0 mm/yr for the northern section based on abundant geomorphic evidence for probable latest Pleistocene and Holocene displacement and, paleoseismic trench investigations that indicate that Quaternary deposits estimated to be between 10 ka and 25 ka, are right laterally offset between about 13 and 25 meters by the Cottonwood Arm segment of the Ortigalita fault. They note the southern segment appears much less active and accordingly, they assign a lower slip rate of 0.2 to 1.0 mm/yr to this segment.
			Southern Ortigalita	60	15 ± 3	90	N/A	SS	7.1	0.2 (0.2) 0.6 (0.6) 1.0 (0.2)	
Ortigalita (cont'd.)		Segmented + Floating Earthquake (0.7)	Northern Ortigalita	40	15 ± 3	90	N/A	SS	6.9	0.5 (0.15) 1.0 (0.35) 2.0 (0.35) 2.5 (0.15)	
			Floating Earthquake on Southern Ortigalita	60	15 ± 3	90	N/A	SS	6.6	0.2 (0.2) 0.6 (0.6) 1.0 (0.2)	
Pittsburgh-Kirby Hills	1.0	Unsegmented (0.4)	N/A	24	20 ± 5	90	N/A	SS	6.7	0.3 (0.4) 0.5 (0.4) 0.7 (0.2)	Characterization from the Thrust Fault Subgroup of the 1999 Working Group.
		Floating Earthquake (0.6)	N/A	N/A	20 ± 5	90	N/A	SS	6.3	0.3 (0.4) 0.5 (0.4) 0.7 (0.2)	
Potrero Hills	0.7	Unsegmented (1.0)	N/A	9	9 ± 2	40 ± 10	SW	R	5.75 (0.3) 6.0 (0.6) 6.25 (0.1)	0.1 (0.2) 0.3 (0.6) 0.6 (0.2)	Characterization based on Unruh and Hector (1999). Fault tip inferred to lie between 0 km and 1 km depth based on analysis of gas well data and construction of geologic cross sections. The fault is assigned a Probability of Activity of (0.7) based on geomorphic and physiographic evidence that slip is being transferred from the active Pittsburg Kirby Hills fault to Wragg Canyon and Hunting Creek-Berryessa fault zones to the north via the Potrero Hills fault.
Pt. Reyes	0.8	Unsegmented	N/A	47	12 ± 3	40 (0.2) 50 (0.6) 60 (0.2)	NE	R	7.0	0.05 (0.2) 0.3 (0.6) 0.5 (0.2)	Cao et al. (2003)
Quien Sabe	1.0	Unsegmented (1.0)	N/A	23	10	90	N/A	SS	6.4	0.1 (0.2) 1.0 (0.6) 2.0 (0.2)	Cao et al. (2003)
San Andreas (Southern)	1.0	Unsegmented (1.0)	N/A	312	12 ± 2	90	N/A	SS	7.8	28 (0.2) 33 (0.6) 38 (0.2)	Characterization from URS.
Sargent	0.8	Unsegmented (1.0)	Sargent	52	15 ± 3	80 ± 10	SW	RO	6.9	1.5 (0.3) 3.0 (0.4) 4.5 (0.3)	Characterization based on WGNCEP (1996). Geodetic measurements indicative of right slip across the southern Sargent fault (Prescott and Burford 1976), evidence for creep of about 3-4 mm/yr, as well as associated historical microseismicity suggest that the Sargent fault is an independent seismic source. The Sargent fault experienced triggered slip during the 1989 M_W 6.9 Loma Prieta earthquake (Aydin 1982). A Probability of Activity of less than 1.0 (0.9) considers that fault slip may occur coseismically as creep or during large magnitude events on the San Andreas fault.

Table 6-1 Bay Area Time-Independent Seismic Source Parameters

Fault Name	Probability of Activity[1]	Rupture Scenario[2]	Segment Name	Rupture Length[3]	Width[4]	Dip[5]	Direction of Dip[6]	Sense of Slip[7]	Magnitude[8]	Slip Rate[9]	Notes
Southeast Extension of Hayward (zone)	1.0	Unsegmented (1.0)	N/A	26	10	90	N/A	SS/RO	6.4	1.0 (0.2) 3.0 (0.6) 5.0 (0.2)	Characterization based on WGNCEP (1996), Graymer et al. (2006), and Fenton and Hitchcock (2001).
Southern Midland	0.8	Unsegmented (1.0)	N/A	26	15 ± 5	70	W	RO	6.6	0.1 (0.3) 0.5 (0.4) 1.0 (0.3)	Activity and rate is inferred from displacement of late Tertiary (and possibly early Pleistocene) strata in seismic reflection profiles (Weber-Band 1994) and apparent displacement of basal peat (Holocene) inferred from analysis of Atwater (1982) data (this study). Tip of fault is inferred by CDOG (1982) to extend above the base of the Tertiary Markley Formation to depths of about 1.5 km, and possibly shallower. Minimum fault depth not constrained by data in CDOG (1982).
Thornton Arch (zone)	0.2	Floating Earthquake (1.0)	N/A	N/A	15 ± 5	70	S (E-W strike)	RO	6.0 (0.3) 6.25 (0.4) 6.5 (0.3)	0.05 (0.3) 0.10.4) 0.15 (0.3)	Possible localization of Quaternary uplift suggesting the presence of active blind fault(s) is inferred based on the deflection of the Mokelumne River north around an arch mapped in the subsurface from oil and gas exploration data (California Division of Oil and Gas 1982). EW strike - based on the orientation of the mapped arch.
Vernalis	0.8	Floating Earthquake (1.0)	N/A	46	15 ± 3	70 ± 10	W	RO	6.25 (0.2) 6.5 (0.4) 6.75 (0.4)	0.07 (0.3) 0.25 (0.4) 0.5 (0.3)	Quaternary activity of the Vernalis fault is inferred from the distribution of older Quaternary deposits (CDMG 1:25,000 San Jose quadrangle) that indicate differential uplift across the fault. Sterling (1992) describes stratigraphic and structural relationships imaged by seismic reflection data indicating "movement as recently as late Pliocene." The slip rate is estimated to be comparable to the estimated rate for the West Tracy fault.
Verona/Williams Thrust System	1.0	Unsegmented (0.6)	N/A	22	21 ± 2	30 (0.1) 45 (0.6) 60 (0.3)	NE	R	6.7	0.1 (0.2) 0.7 (0.5) 1.4 (0.3)	In this model, the Verona/Williams fault is the near surface expression of a deeper east-to northeast-dipping blind thrust fault that underlies the Livermore Valley (Unruh and Sawyer 1997; Sawyer 1998). This model explains fault and fold deformation in the Livermore Valley (including the Los Positas fault, Livermore thrust and Springtown anticline) as secondary structures that either root into the deeper structure or are secondary structures in the hanging wall of the Verona/Williams thrust. These secondary structures are nonseismogenic and are not treated as independent seismic sources. The slip rate distribution is from Savy and Foxall (2002). Fault tip is estimated to be at a depth of 3 km (0.5) or 5 km (0.5).
		Segmented (0.4)	Verona	10	10	30 (0.2) 45 (0.4) 60 (0.4)	NE	R	6.2	0.1 (0.2) 0.7 (0.5) 1.4 (0.3)	Characterization of the fault is based on information summarized in Herd and Brabb (1980), Hart (1980 1981a,b), Jahns and Harding (1982), and source parameters developed by the Thrust Fault Subgroup of Working Group 1999 (WGCEP (2003) subgroup). The total length of the fault is approximately 7-9 km. Field observations and trenching described by Herd and Brabb (1980) provide evidence for late Quaternary surface-rupturing events on the fault. A 5.65-km-long-segment of the fault is included in an Alquist-Priolo zone (Hart 1980, 1981a,b). The slip rate distribution is from Savy and Foxall (2002). Fault tip is estimated to be at a depth of 3 km (0.5) or 5 km (0.5).
			Williams	13	13	30 (0.1) 45 (0.6) 60 (0.3)	NE	R	6.3	0.1 (0.2) 0.3 (0.6) 1.0 (0.2)	Characterization of the fault is based on the following. The total length of the fault is based on mapping by Dibblee (1980, 1981). Carpenter et al. (1984) show the fault as a southwest-vergent thrust fault. The DWR (1979) suggested the fault was active based on displacements observed in Plio-Pleistocene Livermore gravels in the Hetch-Hetchy tunnel and the occurrence of moderate seismicity adjacent to its trace. In the absence of any reported slip rate estimates, a rate of slip comparable to Verona fault is used. Fault tip is estimated to be at a depth of 3 km (0.5) or 5 km (0.5).

Table 6-1 Bay Area Time-Independent Seismic Source Parameters

Fault Name	Probability of Activity[1]	Rupture Scenario[2]	Segment Name	Rupture Length[3]	Width[4]	Dip[5]	Direction of Dip[6]	Sense of Slip[7]	Magnitude[8]	Slip Rate[9]	Notes
			Las Positas P(a) = 0.7	17.5	15 ± 3	90	N/A	SS	6.5	0.1 (0.2) 0.3 (0.6) 1.0 (0.2)	Characterization is based on information summarized by Carpenter et al. (1980,1984) as follows. The total length of ~17.5 km is based on geologic mapping and air photo interpretation. Movement on both southern and northern fault traces extends up into Holocene deposits: faulting may have occurred as recently as 500 to 1,000 years ago. The average slip rate for the north branch of the Las Positas fault zone is 0.4 mm/yr; the range of rates obtained from observed vertical offset and inferred horizontal-to-vertical ratios and age estimates is 0.02 to 0.9 mm/yr.
West Napa	1.0	Unsegmented (0.15)	St. Helena/Dry Creek + West Napa	52	15 ± 3	90	N/A	SS	6.9	1.0 (0.3) 2.0 (0.3) 3.0 (0.3) 4.0 (0.1)	Characterization is based on recent compilation and mapping of the West Napa fault by Hanson and Wesling (2006, 2007) and Clahan et al. (2006) conducted in support of the USGS Quaternary fault database for Northern California (Graymer et al. 2006). The slip rate for the West Napa is not well constrained, but was previously considered to be on the order of 1 mm/yr (1 ± 1 mm/yr, Cao et al. 2003). Several recent studies and observations suggest
		Floating Earthquake (0.35)	N/A	N/A	15 ± 3	90	N/A	SS	6.5	0.5 (0.1) 1.0 (0.3) 2.0 (0.3) 3.0 (0.2) 4/0 (0.1)	the slip rate is higher. These include: 1) more detailed mapping of the fault zone (Hanson and Wesling 2006, 2007) that shows that the fault is better expressed geomorphically than had been recognized previously with evidence for recent (< 600 to 700 years B. P.) displacement; 2) comparison of slip budgets between the regions north and south of Carquinez Strait suggests that a significant amount of slip is being transferred from the North Calaveras fault to the West Napa fault via the Cull Canyon/Laffette/Reliz Valley fault zone; and 3) a recent analysis of GPS data with the preferred model indicating a rate of 4 ± 3 mm/yr (d'Alessio et al. 2005).
		Segmented (0.15)	St. Helena/Dry Creek	24	15 ± 3	90	N/A	SS	6.6	1.0 (0.5) 2.0 (0.2) 3.0 (0.1)	
			West Napa	38	15 ± 3	90	N/A	SS	6.8	1.0 (0.5) 2.0 (0.2) 3.0 (0.1)	
		Segmented + Floating Earthquake (0.35)	Floating Earthquake on West Napa	N/A	15 ± 3	90	N/A	SS	6.4	1.0 (0.5) 2.0 (0.2) 3.0 (0.1)	
			St. Helena/Dry Creek	N/A	15 ± 3	90	N/A	SS	6.4	1.0 (0.5) 2.0 (0.2) 3.0 (0.1)	
		Floating Earthquake (0.9)	N/A	N/A	15 ± 5	70	W	RO	6.0 (0.3) 6.25 (0.4) 6.5 (0.3)	0.1 (0.3) 0.5 (0.4) 1.0 (0.3)	
West Tracy	0.9	Floating Earthquake (1.0)	N/A	30	15 ± 3	70 ± 10	W	RO	6.25 (0.2) 6.5 (0.4) 6.75 (0.4)	0.07 (0.3) 0.25 (0.4) 0.5 (0.3)	Quaternary activity of the West Tracy fault is inferred from the distribution of older Quaternary deposits (CDMG 1:25,000 San Jose quadrangle) that indicate differential uplift across the fault. Very limited data are available to estimate the rate of slip and recent fault behavior. The rate of reverse-oblique slip is inferred to be approximately half the rate estimated for the Midway/Black Butte fault zone. A lower bound of 0.07 mm/yr on the slip rate is estimated based on total vertical separation of about 800 feet (244 meters) of a basal Miocene unconformity across the fault as reported by Sterling (1992), and an assumed duration of deformation (active during the past ~3.5 Ma).
Wragg Canyon	0.7	Unsegmented (1.0)	N/A	17	15 ± 3	90	N/A	SS	6.5	0.1 (0.2) 0.3 (0.6) 0.5 (0.2)	Fault mapped by Sims et al. (1973) along Wragg Canyon; O'Connell et al. (2001) inferred that small earthquakes with strike-slip focal mechanisms are associated with the fault.
Zayente-Vergeles	1.0	Unsegmented (1.0)	N/A	58	12	70 ± 10	SW	R	6.9	0.1 ± 0.1	Cao et al. (2003); Dip information from USGS Quaternary Database

Table 6-2 Bay Area Time-Dependent Seismic Source Parameters

Fault Name	Probability of Activity[1]	Rupture Source[2]	Segment Name	Rupture Length[3]	Width[4]	Dip[5]	Direction of Dip[6]	Sense of Slip[7]	Magnitude[8]	Year	Rate of Characteristic Event[9]			Activity Rate		
											5%	5%	Mean	95%	Mean	95%
		SAS	Santa Cruz Mountains	62	15	90	N/A	SS	6.87	2005:	0.00E+00	4.31E-04	1.79E-03	0.00E+00	1.77E-03	7.34E-03
									7.03	2050:	0.00E+00	2.19E-03	8.26E-03	0.00E+00	9.01E-03	3.39E-02
									7.19	2100:	0.00E+00	4.77E-03	1.92E-02	0.00E+00	1.96E-02	7.90E-02
										2200:	0.00E+00	7.37E-03	3.02E-02	0.00E+00	3.03E-02	1.24E-01
		SAP	Peninsula	85	13	90	N/A	SS	6.97	2005:	0.00E+00	1.31E-03	5.60E-03	0.00E+00	4.32E-03	1.85E-02
									7.15	2050:	0.00E+00	2.61E-03	9.56E-03	0.00E+00	8.63E-03	3.16E-02
									7.31	2100:	0.00E+00	3.71E-03	1.41E-02	0.00E+00	1.23E-02	4.66E-02
										2200:	0.00E+00	4.44E-03	1.64E-02	0.00E+00	1.47E-02	5.43E-02
		SAN	North Coast	191	11	90	N/A	SS	7.30	2005:	0.00E+00	2.12E-04	9.31E-04	0.00E+00	1.15E-03	5.04E-03
									7.45	2050:	0.00E+00	4.14E-04	1.67E-03	0.00E+00	2.24E-03	9.06E-03
									7.59	2100:	0.00E+00	6.07E-04	2.25E-03	0.00E+00	3.29E-03	1.22E-02
										2200:	0.00E+00	8.10E-04	2.99E-03	0.00E+00	4.38E-03	1.62E-02
		SAO	Offshore	135	11	90	N/A	SS	7.13	2005:	0.00E+00	1.80E-04	8.87E-04	0.00E+00	7.50E-04	3.70E-03
									7.29	2050:	0.00E+00	4.04E-04	1.70E-03	0.00E+00	1.69E-03	7.10E-03
									7.44	2100:	0.00E+00	7.08E-04	2.67E-03	0.00E+00	2.96E-03	1.11E-02
										2200:	0.00E+00	1.16E-03	4.33E-03	0.00E+00	4.83E-03	1.81E-02
		SAS+SAP	Peninsula + Santa Cruz Mountains	147		90	N/A	SS	7.28	2005:	3.87E-05	1.01E-03	3.22E-03	2.03E-04	5.33E-03	1.69E-02
									7.42	2050:	1.46E-04	2.06E-03	5.83E-03	7.68E-04	1.08E-02	3.06E-02
									7.55	2100:	2.08E-04	3.14E-03	9.59E-03	1.09E-03	1.65E-02	5.03E-02
										2200:	2.46E-04	4.09E-03	1.28E-02	1.29E-03	2.15E-02	6.69E-02
		SAN+SAO	Offshore + North Coast	326	11	90	N/A	SS	7.55	2005:	2.05E-05	9.43E-04	2.95E-03	1.73E-04	7.96E-03	2.49E-02
									7.70	2050:	2.82E-04	1.65E-03	4.50E-03	2.38E-03	1.40E-02	3.80E-02
									7.83	2100:	4.05E-04	2.35E-03	5.94E-03	3.42E-03	1.98E-02	5.01E-02
										2200:	4.87E-04	3.17E-03	7.99E-03	4.11E-03	2.67E-02	6.74E-02
		SAS+SAP+SAN	North Coast + Peninsula + Santa Cruz Mountains	338	13 ± 3	90	N/A	SS	7.62	2005:	0.00E+00	1.66E-05	8.98E-05	0.00E+00	1.57E-04	8.47E-04
									7.76	2050:	0.00E+00	2.71E-05	1.10E-04	0.00E+00	2.56E-04	1.04E-03
									7.89	2100:	0.00E+00	3.68E-05	1.34E-04	0.00E+00	3.47E-04	1.27E-03
										2200:	0.00E+00	4.64E-05	1.58E-04	0.00E+00	4.38E-04	1.49E-03
		SAP+SAN+SAO	Offshore + North Coast + Peninsula	411	11 ± 2	90	N/A	SS	7.67	2005:	0.00E+00	4.43E-05	2.82E-04	0.00E+00	4.84E-04	3.08E-03
									7.82	2050:	0.00E+00	7.34E-05	4.21E-04	0.00E+00	8.02E-04	4.60E-03
									7.97	2100:	0.00E+00	1.01E-04	4.99E-04	0.00E+00	1.10E-03	5.46E-03
										2200:	0.00E+00	1.31E-04	5.96E-04	0.00E+00	1.43E-03	6.52E-03
		SAS+SAP+SAN+SAO	Offshore + North Coast + Peninsula + Santa Cruz Mountains (1906)	473	13 ± 2	90	N/A	SS	7.75	2005:	7.82E-05	1.46E-03	4.25E-03	9.74E-04	1.81E-02	5.30E-02
									7.90	2050:	5.97E-04	2.30E-03	6.16E-03	7.44E-03	2.86E-02	7.66E-02
									8.06	2100:	1.03E-03	3.08E-03	7.74E-03	1.29E-02	3.83E-02	9.63E-02
										2200:	1.31E-03	3.94E-03	9.02E-03	1.64E-02	4.90E-02	1.12E-01
		Floating Earthquake	N/A	N/A	13 ± 3	90	N/A	SS	6.9	2005:	1.62E-04	1.81E-03	6.49E-03	3.87E-04	4.33E-03	1.55E-02
										2050:	1.99E-04	3.72E-03	1.32E-02	4.76E-04	8.89E-03	3.16E-02
										2100:	2.09E-04	5.80E-03	2.14E-02	5.00E-04	1.39E-02	5.12E-02
										2200:	2.12E-04	8.03E-03	3.12E-02	5.07E-04	1.92E-02	7.45E-02

Table 6-2 Bay Area Time-Dependent Seismic Source Parameters

Fault Name	Probability of Activity[1]	Rupture Source[2]	Segment Name	Rupture Length[3]	Width[4]	Dip[5]	Direction of Dip[6]	Sense of Slip[7]	Magnitude[8]	Year	Rate of Characteristic Event[9]			Activity Rate		
											5%	5%	Mean	95%	Mean	95%
Hayward – Rodgers Creek	1.0	HS	Southern Hayward	53	12 ± 2	90	N/A	SS	6.42 6.67 6.90	2005: 2050: 2100: 2200:	8.66E-04 1.15E-03 1.28E-03 1.38E-03	4.24E-03 5.13E-03 5.75E-03 6.41E-03	1.08E-02 1.28E-02 1.48E-02 1.65E-02	1.56E-03 2.06E-03 2.31E-03 2.49E-03	7.63E-03 9.23E-03 1.04E-02 1.15E-02	1.95E-02 2.31E-02 2.66E-02 2.96E-02
		HN	North Hayward	35	12 ± 2	90	N/A	SS	6.20 6.49 6.73	2005: 2050: 2100: 2200:	9.57E-04 1.05E-03 1.14E-03 1.20E-03	5.17E-03 5.48E-03 5.75E-03 6.06E-03	1.46E-02 1.54E-02 1.57E-02 1.64E-02	1.44E-03 1.58E-03 1.72E-03 1.81E-03	7.77E-03 8.25E-03 8.66E-03 9.13E-03	2.19E-02 2.32E-02 2.37E-02 2.47E-02
		HS+HN	Hayward	88	12 ± 2	90	N/A	SS	6.71 6.90 7.09	2005: 2050: 2100: 2200:	7.36E-04 8.37E-04 9.21E-04 1.02E-03	3.38E-03 3.88E-03 4.26E-03 4.67E-03	8.65E-03 1.03E-02 1.14E-02 1.28E-02	1.72E-03 1.96E-03 2.16E-03 2.38E-03	7.91E-03 9.10E-03 9.97E-03 1.10E-02	2.03E-02 2.42E-02 2.66E-02 3.01E-02
		RC	Rodgers Creek	63	12 ± 2	90	N/A	SS	6.83 6.98 7.14	2005: 2050: 2100: 2200:	1.56E-03 1.72E-03 1.89E-03 2.23E-03	5.93E-03 6.49E-03 6.97E-03 7.59E-03	1.44E-02 1.71E-02 1.88E-02 2.07E-02	4.16E-03 4.58E-03 5.05E-03 5.93E-03	1.58E-02 1.73E-02 1.86E-02 2.02E-02	3.85E-02 4.56E-02 5.02E-02 5.50E-02
		HN+RC	North Hayward + Rodgers Creek	98	12 ± 2	90	N/A	SS	6.96 7.11 7.27	2005: 2050: 2100: 2200:	4.10E-05 4.49E-05 4.91E-05 4.91E-05	7.60E-04 8.25E-04 8.81E-04 9.50E-04	2.34E-03 2.53E-03 2.78E-03 2.97E-03	1.29E-04 1.41E-04 1.54E-04 1.54E-04	2.38E-03 2.59E-03 2.76E-03 2.98E-03	7.35E-03 7.95E-03 8.73E-03 9.32E-03
		HS+HN+RC	Hayward + Rodgers Creek	151	12 ± 2	90	N/A	SS	7.11 7.26 7.40	2005: 2050: 2100: 2200:	6.14E-05 6.76E-05 7.33E-05 7.95E-05	4.11E-04 4.59E-04 4.98E-04 5.44E-04	1.11E-03 1.32E-03 1.43E-03 1.63E-03	2.39E-04 2.64E-04 2.86E-04 3.10E-04	1.60E-03 1.79E-03 1.94E-03 2.12E-03	4.35E-03 5.14E-03 5.60E-03 6.37E-03
		Floating Earthquake	N/A	N/A	12 ± 2	90	N/A	SS	6.90	2005: 2050: 2100: 2200:	1.02E-04 1.09E-04 1.19E-04 1.35E-04	2.52E-04 2.59E-04 2.70E-04 2.90E-04	4.80E-04 4.85E-04 4.94E-04 5.46E-04	2.44E-04 2.61E-04 2.84E-04 3.23E-04	6.02E-04 6.20E-04 6.45E-04 6.94E-04	1.15E-03 1.16E-03 1.18E-03 1.30E-03
Calaveras	1.0	CS	Southern Calaveras	19	11 ± 2	90	N/A	SS	0.0 5.79 6.12	2005: 2050: 2100: 2200:	0.00E+00 0.00E+00 0.00E+00 0.00E+00	1.17E-02 1.21E-02 1.25E-02 1.30E-02	3.77E-02 4.03E-02 4.15E-02 4.24E-02	0.00E+00 0.00E+00 0.00E+00 0.00E+00	1.60E-02 1.66E-02 1.70E-02 1.78E-02	5.15E-02 5.52E-02 5.68E-02 5.80E-02
		CC	Central Calaveras	59	11 ± 2	90	N/A	SS	5.79 6.23 6.61	2005: 2050: 2100: 2200:	8.25E-04 1.97E-03 2.10E-03 2.38E-03	6.40E-03 8.52E-03 9.12E-03 9.57E-03	1.80E-02 2.49E-02 2.63E-02 2.70E-02	1.00E-03 2.40E-03 2.55E-03 2.90E-03	7.78E-03 1.04E-02 1.11E-02 1.16E-02	2.19E-02 3.03E-02 3.20E-02 3.29E-02
		CS+CC	South + Central Calaveras	78	11 ± 2	90	N/A	SS	5.93 6.36 6.68	2005: 2050: 2100: 2200:	0.00E+00 0.00E+00 0.00E+00 0.00E+00	2.16E-03 2.74E-03 2.94E-03 3.09E-03	7.92E-03 1.01E-02 1.09E-02 1.14E-02	0.00E+00 0.00E+00 0.00E+00 0.00E+00	2.85E-03 3.61E-03 3.88E-03 4.08E-03	1.04E-02 1.33E-02 1.44E-02 1.50E-02
		CN	Northern Calaveras	45	13 ± 2	90	N/A	SS	6.62 6.78 6.93	2005: 2050: 2100: 2200:	1.10E-03 1.23E-03 1.35E-03 1.56E-03	5.14E-03 5.50E-03 5.82E-03 6.26E-03	1.45E-02 1.57E-02 1.68E-02 1.81E-02	2.28E-03 2.54E-03 2.79E-03 3.23E-03	1.06E-02 1.14E-02 1.20E-02 1.30E-02	3.00E-02 3.26E-02 3.48E-02 3.74E-02
		CC+CN	Central + Northern Calaveras	104	13 ± 2	90	N/A	SS	6.72 6.91 7.08	2005: 2050: 2100: 2200:	0.00E+00 0.00E+00 0.00E+00 0.00E+00	1.37E-04 1.65E-04 1.81E-04 1.97E-04	1.00E-03 1.14E-03 1.28E-03 1.36E-03	0.00E+00 0.00E+00 0.00E+00 0.00E+00	3.24E-04 3.91E-04 4.28E-04 4.67E-04	2.37E-03 2.70E-03 3.02E-03 3.21E-03

Table 6-2 Bay Area Time-Dependent Seismic Source Parameters

Fault Name	Probability of Activity[1]	Rupture Source[2]	Segment Name	Rupture Length[3]	Width[4]	Dip[5]	Direction of Dip[6]	Sense of Slip[7]	Magnitude[8]	Year	Rate of Characteristic Event[9]			Activity Rate		
											5%	5%	Mean	95%	Mean	95%
Calaveras (cont'd.)		CS+CC+CN	Northern + Central + Southern Calaveras	123	11 ± 2	90	N/A	SS	6.76 6.94 7.11	2005: 2050: 2100: 2200:	0.00E+00 0.00E+00 0.00E+00 0.00E+00	8.05E-04 9.38E-04 1.00E-03 1.07E-03	2.81E-03 3.40E-03 3.58E-03 3.71E-03	0.00E+00 0.00E+00 0.00E+00 0.00E+00	1.99E-03 2.32E-03 2.48E-03 2.65E-03	6.96E-03 8.42E-03 8.85E-03 9.17E-03
		Floating Earthquake	N/A	N/A	11 ± 2	90	N/A	SS	6.2	2005: 2050: 2100: 2200:	6.17E-04 6.92E-04 7.43E-04 8.39E-04	2.63E-03 2.73E-03 2.85E-03 3.11E-03	6.66E-03 6.67E-03 6.88E-03 7.86E-03	7.83E-04 8.78E-04 9.43E-04 1.06E-03	3.34E-03 3.46E-03 3.62E-03 3.95E-03	8.45E-03 8.47E-03 8.73E-03 9.98E-03
		Floating Earthquake on CS+CC	N/A	N/A	11 ± 2	90	N/A	SS	6.2	2005: 2050: 2100: 2200:	2.10E-03 2.22E-03 2.37E-03 2.55E-03	1.04E-02 1.07E-02 1.13E-02 1.23E-02	2.50E-02 2.51E-02 2.64E-02 2.88E-02	2.66E-03 2.81E-03 3.00E-03 3.24E-03	1.32E-02 1.36E-02 1.43E-02 1.56E-02	3.17E-02 3.18E-02 3.35E-02 3.66E-02
Concord – Green Valley	1.0	CON	Concord	20	16 ± 2	90	N/A	SS	5.79 6.25 6.65	2005: 2050: 2100: 2200:	1.56E-04 2.02E-04 2.21E-04 2.66E-04	1.88E-03 2.06E-03 2.21E-03 2.41E-03	5.70E-03 6.03E-03 6.63E-03 7.06E-03	1.91E-04 2.47E-04 2.70E-04 3.25E-04	2.30E-03 2.51E-03 2.70E-03 2.94E-03	6.97E-03 7.36E-03 8.10E-03 8.63E-03
		GVS	Southern Green Valley	22	14 ± 2	90	N/A	SS	5.81 6.24 6.60	2005: 2050: 2100: 2200:	6.22E-05 8.50E-05 9.77E-05 1.16E-04	8.78E-04 9.57E-04 1.02E-03 1.11E-03	2.85E-03 3.08E-03 3.20E-03 3.49E-03	7.57E-05 1.03E-04 1.19E-04 1.41E-04	1.07E-03 1.16E-03 1.25E-03 1.35E-03	3.47E-03 3.75E-03 3.90E-03 4.25E-03
		CON+GVS	Concord + Southern Green Valley	42	14 ± 2	90	N/A	SS	6.20 6.58 6.87	2005: 2050: 2100: 2200:	2.78E-05 3.28E-05 4.30E-05 5.32E-05	5.99E-04 6.52E-04 6.99E-04 7.60E-04	2.00E-03 2.13E-03 2.29E-03 2.52E-03	4.42E-05 5.23E-05 6.85E-05 8.47E-05	9.54E-04 1.04E-03 1.11E-03 1.21E-03	3.19E-03 3.40E-03 3.64E-03 4.01E-03
		GVN	Northern Green Valley	14	14 ± 2	90	N/A	SS	5.56 6.02 6.43	2005: 2050: 2100: 2200:	1.98E-04 2.33E-04 2.73E-04 3.14E-04	2.36E-03 2.55E-03 2.71E-03 2.92E-03	7.05E-03 7.56E-03 7.66E-03 8.23E-03	2.17E-04 2.55E-04 3.00E-04 3.45E-04	2.59E-03 2.80E-03 2.98E-03 3.21E-03	7.74E-03 8.31E-03 8.41E-03 9.04E-03
		GVS+GVN	Green Valley	36	14 ± 2	90	N/A	SS	6.11 6.48 6.77	2005: 2050: 2100: 2200:	8.35E-05 1.03E-04 1.18E-04 1.39E-04	1.20E-03 1.31E-03 1.40E-03 1.52E-03	3.78E-03 4.23E-03 4.41E-03 4.81E-03	1.22E-04 1.51E-04 1.72E-04 2.04E-04	1.76E-03 1.92E-03 2.05E-03 2.22E-03	5.53E-03 6.19E-03 6.44E-03 7.03E-03
		CON+GVS+GVN	Concord+Green Valley	56	14 ± 2	90	N/A	SS	6.42 6.71 6.95	2005: 2050: 2100: 2200:	2.53E-04 3.06E-04 3.70E-04 4.63E-04	2.32E-03 2.57E-03 2.77E-03 3.05E-03	7.37E-03 7.91E-03 8.24E-03 8.76E-03	4.67E-04 5.64E-04 6.82E-04 8.54E-04	4.27E-03 4.73E-03 5.11E-03 5.62E-03	1.36E-02 1.46E-02 1.52E-02 1.62E-02
		Floating Earthquake	N/A	N/A	14 ± 2	90	N/A	SS	6.2	2005: 2050: 2100: 2200:	1.06E-04 1.18E-04 1.23E-04 1.32E-04	2.40E-03 2.47E-03 2.56E-03 2.74E-03	1.07E-02 1.08E-02 1.10E-02 1.13E-02	1.36E-04 1.51E-04 1.57E-04 1.69E-04	3.07E-03 3.16E-03 3.28E-03 3.51E-03	1.37E-02 1.39E-02 1.41E-02 1.44E-02
San Gregorio	1.0	SGS	Southern San Gregorio	66	12 ± 2	90	N/A	SS	6.76 6.96 7.12	2005: 2050: 2100: 2200:	0.00E+00 0.00E+00 0.00E+00 0.00E+00	8.17E-04 8.96E-04 9.75E-04 1.11E-03	3.09E-03 3.33E-03 3.58E-03 3.83E-03	0.00E+00 0.00E+00 0.00E+00 0.00E+00	2.04E-03 2.24E-03 2.43E-03 2.77E-03	7.71E-03 8.32E-03 8.94E-03 9.55E-03
		SGN	Northern San Gregorio	110	13 ± 2	90	N/A	SS	7.07 7.23 7.40	2005: 2050: 2100: 2200:	0.00E+00 0.00E+00 0.00E+00 0.00E+00	1.41E-03 1.58E-03 1.73E-03 1.97E-03	5.03E-03 5.45E-03 5.81E-03 6.23E-03	0.00E+00 0.00E+00 0.00E+00 0.00E+00	5.42E-03 6.06E-03 6.66E-03 7.58E-03	1.93E-02 2.09E-02 2.23E-02 2.39E-02

Table 6-2 Bay Area Time-Dependent Seismic Source Parameters

Fault Name	Probability of Activity[1]	Rupture Source[2]	Segment Name	Rupture Length[3]	Width[4]	Dip[5]	Direction of Dip[6]	Sense of Slip[7]	Magnitude[8]	Year	Rate of Characteristic Event[9]			Activity Rate		
											5%	5%	Mean	95%	Mean	95%
San Gregorio (cont'd.)		SGS+SGN	Northern + Southern San Gregorio						7.30 7.44 7.58	2005: 2050: 2100: 2200:	0.00E+00 0.00E+00 0.00E+00 0.00E+00	9.22E-04 1.03E-03 1.15E-03 1.33E-03	2.93E-03 3.33E-03 3.52E-03 4.01E-03	0.00E+00 0.00E+00 0.00E+00 0.00E+00	4.94E-03 5.51E-03 6.16E-03 7.13E-03	1.57E-02 1.78E-02 1.89E-02 2.15E-02
		Floating Earthquake	N/A	N/A	13 ± 2	90	N/A	SS	6.9	2005: 2050: 2100: 2200:	3.05E-04 3.21E-04 3.34E-04 3.50E-04	7.23E-04 7.45E-04 7.76E-04 8.37E-04	1.23E-03 1.24E-03 1.25E-03 1.45E-03	7.35E-04 7.73E-04 8.04E-04 8.44E-04	1.74E-03 1.79E-03 1.87E-03 2.02E-03	2.96E-03 2.99E-03 3.02E-03 3.49E-03
Greenville	1.0	GS	Southern Greenville	24	15 ± 3	90	N/A	SS	6.40 6.60 6.78	2005: 2050: 2100: 2200:	3.26E-05 9.32E-05 1.91E-04 3.30E-04	1.08E-03 1.19E-03 1.31E-03 1.51E-03	2.80E-03 2.90E-03 3.08E-03 3.44E-03	5.46E-05 1.56E-04 3.20E-04 5.52E-04	1.81E-03 1.99E-03 2.19E-03 2.53E-03	4.69E-03 4.85E-03 5.16E-03 5.76E-03
		GN	Northern Greenville	27	15 ± 3	90	N/A	SS	6.45 6.66 6.84	2005: 2050: 2100: 2200:	1.16E-05 6.08E-05 1.39E-04 2.32E-04	1.03E-03 1.12E-03 1.23E-03 1.43E-03	2.82E-03 2.80E-03 3.14E-03 3.67E-03	2.06E-05 1.08E-04 2.46E-04 4.11E-04	1.82E-03 1.98E-03 2.18E-03 2.53E-03	4.99E-03 4.96E-03 5.57E-03 6.50E-03
		GS+GN	Southern+Northern Greenville	51	15 ± 3	90	N/A	SS	6.78 6.94 7.11	2005: 2050: 2100: 2200:	9.29E-05 1.16E-04 1.38E-04 1.75E-04	5.32E-04 5.79E-04 6.38E-04 7.40E-04	1.29E-03 1.36E-03 1.48E-03 1.71E-03	2.34E-04 2.93E-04 3.49E-04 4.42E-04	1.34E-03 1.46E-03 1.61E-03 1.87E-03	3.26E-03 3.43E-03 3.73E-03 4.31E-03
		Floating Earthquake	N/A	N/A	15 ± 3	90	N/A	SS	6.2	2005: 2050: 2100: 2200:	5.82E-05 6.17E-05 6.37E-05 6.55E-05	1.49E-04 1.54E-04 1.60E-04 1.72E-04	2.73E-04 2.74E-04 2.85E-04 3.20E-04	7.44E-05 7.89E-05 8.15E-05 8.38E-05	1.91E-04 1.96E-04 2.04E-04 2.20E-04	3.49E-04 3.50E-04 3.64E-04 4.10E-04
Mt Diablo	1.0	MTD	Mt. Diablo	31	17 ± 2	30 (0.2) 45 (0.6) 50 (0.2)	NE	R	6.48 6.65 6.83	2005: 2050: 2100: 2200:	3.97E-04 5.52E-04 6.16E-04 6.64E-04	2.71E-03 2.97E-03 3.23E-03 3.66E-03	6.72E-03 7.45E-03 7.89E-03 8.99E-03	7.07E-04 9.84E-04 1.10E-03 1.18E-03	4.84E-03 5.29E-03 5.75E-03 6.53E-03	1.20E-02 1.33E-02 1.41E-02 1.60E-02

Table 6-3 Mean Expert Weights for Probability Models Applied to the SFBR Fault Systems (Table 5.5, WGCEP 2003)

Fault System	Poisson	Empirical	BPT	BPT-step	Time-Predictable
San Andreas	0.100	0.181	0.154	0.231	0.335
Hayward/Rodger's Creek	0.123	0.285	0.131	0.462	—
Calaveras	0.227	0.315	0.142	0.315	—
Concord/Green Valley	0.246	0.277	0.123	0.354	—
San Gregorio	0.196	0.292	0.115	0.396	—
Greenville	0.231	0.288	0.131	0.350	—
Mt. Diablo Thrust	0.308	0.396	0.092	0.204	—

Table 6-4 Empirical Model Factors

Model	Extrapolated Annual Number of Events for Year:			
	2005	**2055**	**2105**	**2205**
A	0.014	0.014	0.014	0.014
B	0.016	0.016	0.016	0.016
C	0.011	0.011	0.011	0.011
D	0.020	0.020	0.020	0.020
E	0.016	0.018	0.020	0.025
F	0.018	0.026	0.034	0.050
Empirical Factors Based on Long Term Rate of 0.031				
Minimum	0.355	0.355	0.355	0.355
Average	0.512	0.567	0.622	0.733
Maximum	0.645	0.850	1.107	1.623

Table 6-5 Ground Motions with a 2% Exceedance Probability in 50 Years (2,500-Year Return Period)

Peak Ground Acceleration (g)

	TI	2005	2050	2100	2200
Sherman Island	0.64	0.64	0.64	0.64	0.65
Clifton Court	0.66	0.66	0.66	0.66	0.67
Montezuma Slough	0.75	0.74	0.74	0.74	0.75
Delta Cross Channel	0.38	0.37	0.37	0.37	0.37
Stockton	0.33	0.32	0.32	0.32	0.33
Sacramento	0.30	0.30	0.30	0.30	0.30

1.0 Sec Spectral Acceleration (g)

	TI	2005	2050	2100	2200
Sherman Island	0.77	0.77	0.78	0.79	0.80
Clifton Court	0.82	0.82	0.83	0.84	0.85
Montezuma Slough	0.91	0.90	0.90	0.91	0.93
Delta Cross Channel	0.48	0.48	0.49	0.49	0.50
Stockton	0.45	0.44	0.45	0.46	0.47
Sacramento	0.43	0.42	0.43	0.43	44

TI = Time-Independent

Table 6-6 Distribution of Probability of Failure – Sample Results

Vulnerability Class Index	Initial Freeboard (ft)	Earthquake Magnitude	Epistemic Cumulative % Prob.	Probability of Failure for Given Ground Motion Level										
				0.05	0.1	0.2	0.3	0.4	0.5	0.6	0.7	0.8	0.9	1
1	4	5.5	50%	0.0038	0.0038	0.0038	1	1	1	1	1	1	1	1
1	4	6.5	50%	0.0038	0.0038	1	1	1	1	1	1	1	1	1
1	4	7.5	50%	0.0038	1	1	1	1	1	1	1	1	1	1
2	4	5.5	50%	0.0038	0.0038	0.0038	1	1	1	1	1	1	1	1
2	4	6.5	50%	0.0038	0.0038	1	1	1	1	1	1	1	1	1
2	4	7.5	50%	0.0038	1	1	1	1	1	1	1	1	1	1
3	4	5.5	50%	0.0038	0.0038	0.0038	1	1	1	1	1	1	1	1
3	4	6.5	50%	0.0038	0.0038	1	1	1	1	1	1	1	1	1
3	4	7.5	50%	0.0038	1	1	1	1	1	1	1	1	1	1
4	4	5.5	50%	0.0039	0.0039	0.0039	1	1	1	1	1	1	1	1
4	4	6.5	50%	0.0039	0.0039	1	1	1	1	1	1	1	1	1
4	4	7.5	50%	0.0039	1	1	1	1	1	1	1	1	1	1
5	4	5.5	50%	0.0038	0.0038	0.0038	1	1	1	1	1	1	1	1
5	4	6.5	50%	0.0038	0.0038	1	1	1	1	1	1	1	1	1
5	4	7.5	50%	0.0038	1	1	1	1	1	1	1	1	1	1
6	4	5.5	50%	0.0020	0.0044	0.0201	0.0920	0.4219	1	1	1	1	1	1
6	4	6.5	50%	0.0138	0.0295	0.1353	0.6204	1	1	1	1	1	1	1
6	4	7.5	50%	0.0929	0.1989	0.9124	1	1	1	1	1	1	1	1
7	4	5.5	50%	0.0018	0.0037	0.0163	0.0714	0.3120	1	1	1	1	1	1
7	4	6.5	50%	0.0118	0.0246	0.1074	0.4694	1	1	1	1	1	1	1
7	4	7.5	50%	0.0773	0.1616	0.7061	1	1	1	1	1	1	1	1
8	4	5.5	50%	0.0027	0.0047	0.0142	0.0434	0.1321	0.4026	1	1	1	1	1
8	4	6.5	50%	0.0115	0.0201	0.0611	0.1863	0.5679	1	1	1	1	1	1
8	4	7.5	50%	0.0494	0.0862	0.2628	0.8009	1	1	1	1	1	1	1
9	4	5.5	50%	0.0013	0.0025	0.0096	0.0365	0.1390	0.5291	1	1	1	1	1
9	4	6.5	50%	0.0075	0.0146	0.0555	0.2113	0.8048	1	1	1	1	1	1
9	4	7.5	50%	0.0433	0.0844	0.3214	1	1	1	1	1	1	1	1
10	4	5.5	50%	0.0009	0.0017	0.0068	0.0267	0.1055	0.4162	1	1	1	1	1
10	4	6.5	50%	0.0054	0.0108	0.0426	0.1681	0.6635	1	1	1	1	1	1
10	4	7.5	50%	0.0342	0.0679	0.2680	1	1	1	1	1	1	1	1
11	4	5.5	50%	0.0007	0.0013	0.0046	0.0162	0.0567	0.1991	0.6991	1	1	1	1

Table 6-6 Distribution of Probability of Failure – Sample Results

Vulnerability Class Index	Initial Freeboard (ft)	Earthquake Magnitude	Epistemic Cumulative % Prob.	Probability of Failure for Given Ground Motion Level										
				0.05	0.1	0.2	0.3	0.4	0.5	0.6	0.7	0.8	0.9	1
11	4	6.5	50%	0.0036	0.0067	0.0235	0.0823	0.2890	1	1	1	1	1	1
11	4	7.5	50%	0.0182	0.0340	0.1195	0.4194	1	1	1	1	1	1	1
12	4	5.5	50%	0.0003	0.0006	0.0021	0.0074	0.0265	0.0951	0.3410	1	1	1	1
12	4	6.5	50%	0.0017	0.0032	0.0115	0.0414	0.1484	0.5320	1	1	1	1	1
12	4	7.5	50%	0.0095	0.0180	0.0646	0.2315	0.8300	1	1	1	1	1	1
13	4	5.5	50%	0.0002	0.0004	0.0015	0.0055	0.0195	0.0698	0.2496	0.8928	1	1	1
13	4	6.5	50%	0.0013	0.0026	0.0091	0.0326	0.1167	0.4175	1	1	1	1	1
13	4	7.5	50%	0.0081	0.0153	0.0546	0.1953	0.6984	1	1	1	1	1	1
14	4	5.5	50%	0.0002	0.0004	0.0013	0.0043	0.0144	0.0475	0.1567	0.5177	1	1	1
14	4	6.5	50%	0.0010	0.0018	0.0060	0.0198	0.0654	0.2162	0.7140	1	1	1	1
14	4	7.5	50%	0.0046	0.0083	0.0273	0.0903	0.2981	0.9847	1	1	1	1	1
15	4	5.5	50%	0.0000	0.0000	0.0000	0.0000	0.0000	0.0001	0.0003	0.0008	0.0021	0.0058	0.0162
15	4	6.5	50%	0.0000	0.0000	0.0000	0.0001	0.0002	0.0006	0.0018	0.0049	0.0136	0.0377	0.1046
15	4	7.5	50%	0.0000	0.0001	0.0002	0.0005	0.0015	0.0041	0.0114	0.0316	0.0876	0.2429	0.6739
16	4	5.5	50%	0.0000	0.0000	0.0001	0.0003	0.0010	0.0039	0.0151	0.0580	0.2236	0.8620	1
16	4	6.5	50%	0.0001	0.0001	0.0005	0.0020	0.0076	0.0292	0.1125	0.4335	1	1	1
16	4	7.5	50%	0.0005	0.0010	0.0038	0.0147	0.0566	0.2180	0.8402	1	1	1	1
17	4	5.5	50%	0.0000	0.0001	0.0002	0.0007	0.0025	0.0089	0.0317	0.1130	0.4027	1	1
17	4	6.5	50%	0.0002	0.0004	0.0013	0.0045	0.0159	0.0568	0.2024	0.7210	1	1	1
17	4	7.5	50%	0.0012	0.0022	0.0080	0.0285	0.1017	0.3623	1	1	1	1	1
18	4	5.5	50%	0.0002	0.0004	0.0013	0.0039	0.0121	0.0372	0.1144	0.3520	1	1	1
18	4	6.5	50%	0.0013	0.0023	0.0070	0.0216	0.0664	0.2041	0.6280	1	1	1	1
18	4	7.5	50%	0.0071	0.0125	0.0385	0.1184	0.3642	1	1	1	1	1	1
19	4	5.5	50%	0.0036	0.0037	0.0037	0.0038	0.0038	0.0039	0.0040	0.0040	0.0041	0.0042	0.0042
19	4	6.5	50%	0.0038	0.0038	0.0039	0.0040	0.0040	0.0041	0.0042	0.0042	0.0043	0.0044	0.0044
19	4	7.5	50%	0.0040	0.0040	0.0041	0.0041	0.0042	0.0043	0.0043	0.0044	0.0045	0.0046	0.0046
20	4	5.5	50%	0.0000	0.0000	0.0000	0.0000	0.0000	0.0000	0.0002	0.0012	0.0062	0.0321	0.1661
20	4	6.5	50%	0.0000	0.0000	0.0000	0.0000	0.0001	0.0006	0.0032	0.0167	0.0866	0.4484	1
20	4	7.5	50%	0.0000	0.0000	0.0001	0.0003	0.0017	0.0087	0.0451	0.2338	1	1	1
21	4	5.5	50%	0.0000	0.0000	0.0000	0.0000	0.0002	0.0010	0.0044	0.0197	0.0884	0.3970	1
21	4	6.5	50%	0.0000	0.0000	0.0001	0.0004	0.0017	0.0078	0.0352	0.1580	0.7098	1	1

Table 6-6 Distribution of Probability of Failure – Sample Results

Vulnerability Class Index	Initial Freeboard (ft)	Earthquake Magnitude	Epistemic Cumulative % Prob.	Probability of Failure for Given Ground Motion Level										
				0.05	**0.1**	**0.2**	**0.3**	**0.4**	**0.5**	**0.6**	**0.7**	**0.8**	**0.9**	**1**
21	4	7.5	50%	0.0001	0.0002	0.0007	0.0031	0.0140	0.0629	0.2825	1	1	1	1
22	4	5.5	50%	0.0001	0.0001	0.0003	0.0010	0.0029	0.0089	0.0274	0.0838	0.2567	0.7864	1
22	4	6.5	50%	0.0003	0.0006	0.0017	0.0053	0.0163	0.0499	0.1528	0.4682	1	1	1
22	4	7.5	50%	0.0018	0.0032	0.0097	0.0297	0.0910	0.2788	0.8540	1	1	1	1
23	4	5.5	50%	0.0072	0.0095	0.0167	0.0293	0.0515	0.0904	0.1588	0.2789	0.4897	0.8599	1
23	4	6.5	50%	0.0107	0.0142	0.0250	0.0439	0.0771	0.1354	0.2378	0.4176	0.7333	1	1
23	4	7.5	50%	0.0161	0.0213	0.0374	0.0658	0.1155	0.2028	0.3561	0.6253	1	1	1
24	4	5.5	50%	0.0073	0.0095	0.0159	1	1	1	1	1	1	1	1
24	4	6.5	50%	0.0108	0.0139	1	1	1	1	1	1	1	1	1
24	4	7.5	50%	0.0157	1	1	1	1	1	1	1	1	1	1

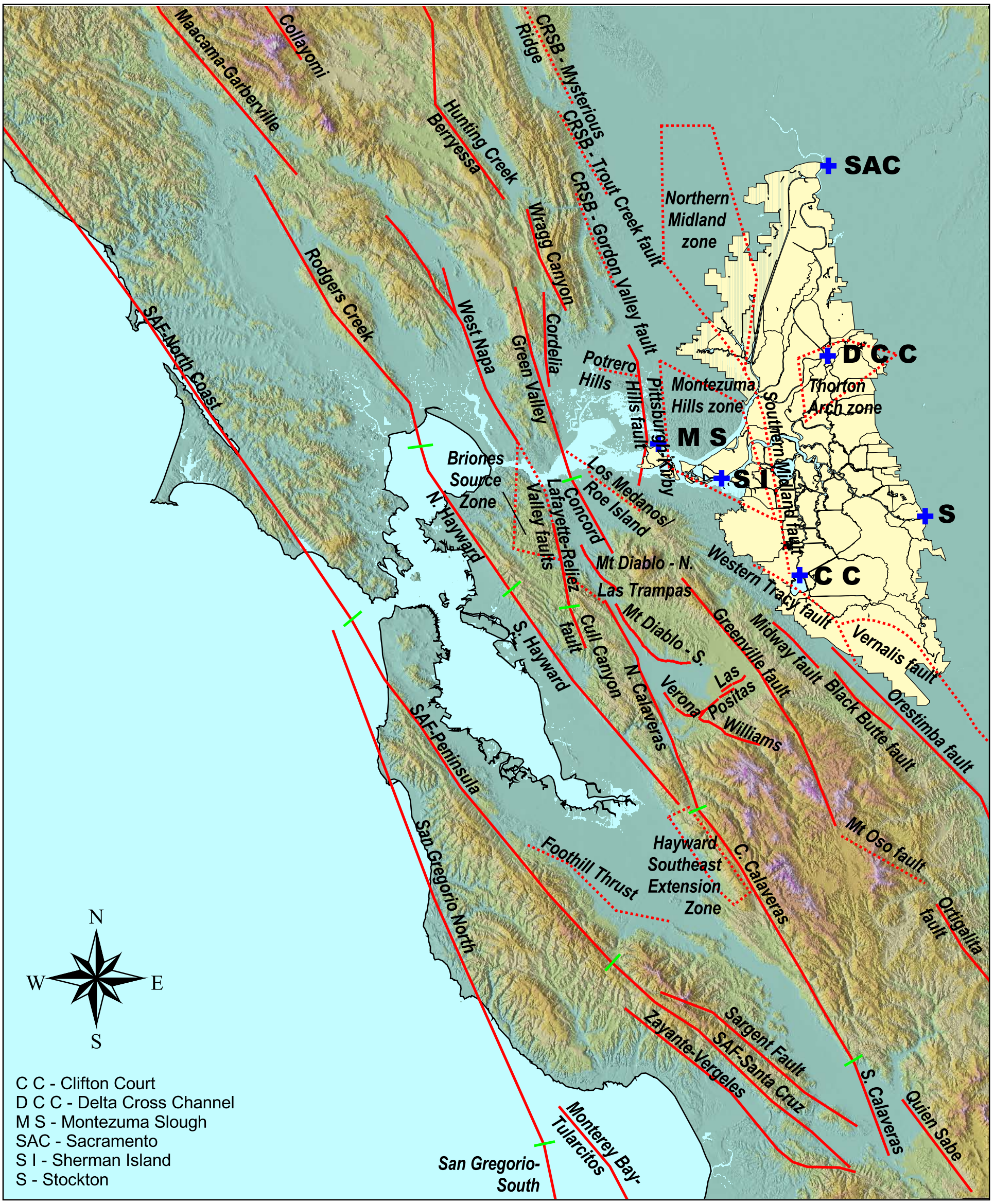

URS	Delta Risk Management Strategy, California Project No. 26815431	FAULTS IN THE SAN FRANCISCO BAY REGION	Figure 6-1

URS	Delta Risk Management Strategy, California Project No. 26815431	ACTIVE FAULTS IN THE SITE REGION	Figure 6-2

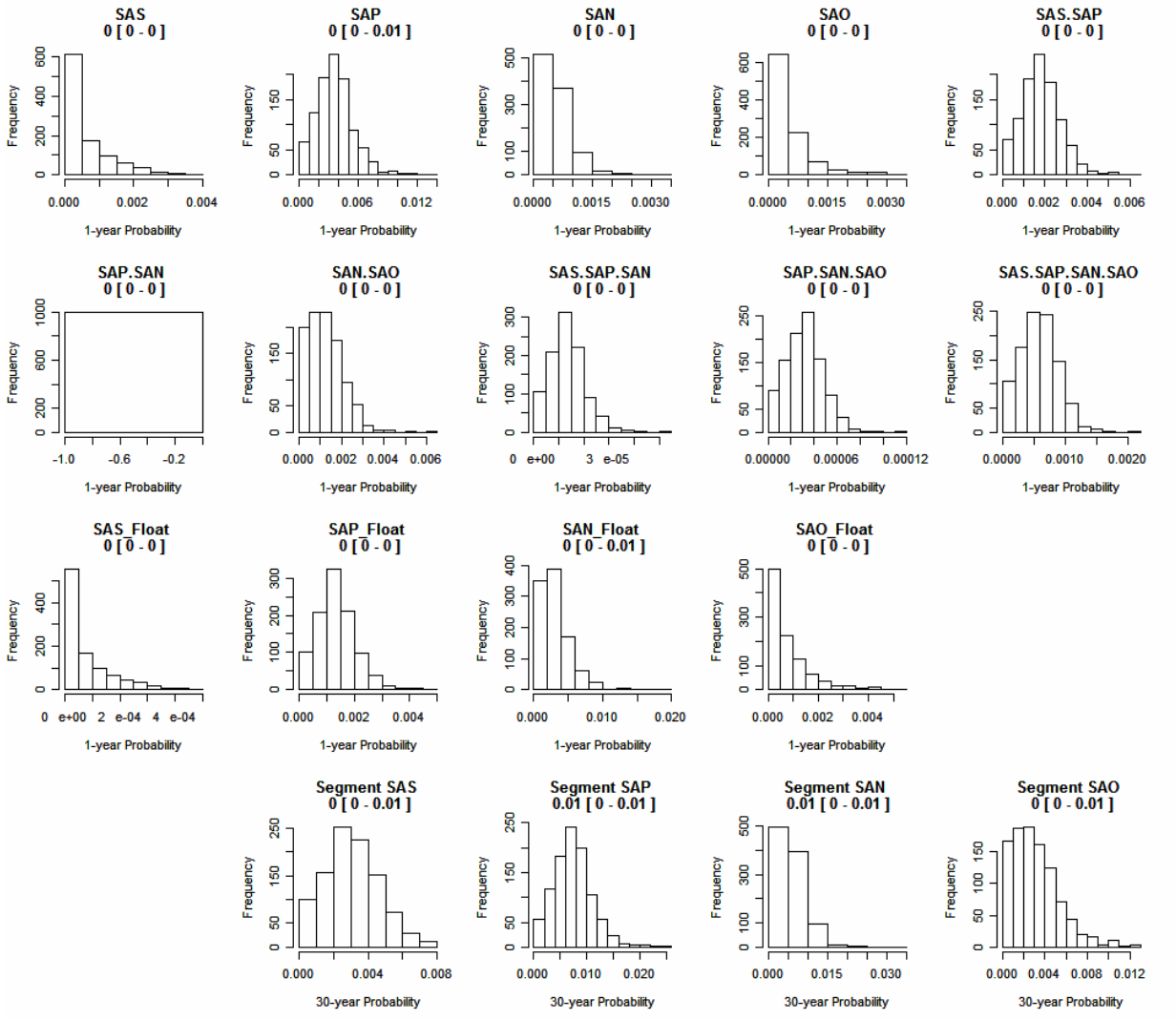

URS	DELTA RISK MANAGEMENT STRATEGY California	Time-Dependent Probabilities for the San Andreas Rupture Scenarios for 2005	Figure 6-3
	Project No. 26815621		

Delta Risk\Figures\TimePred2005.grf 1/31/073:45 PM

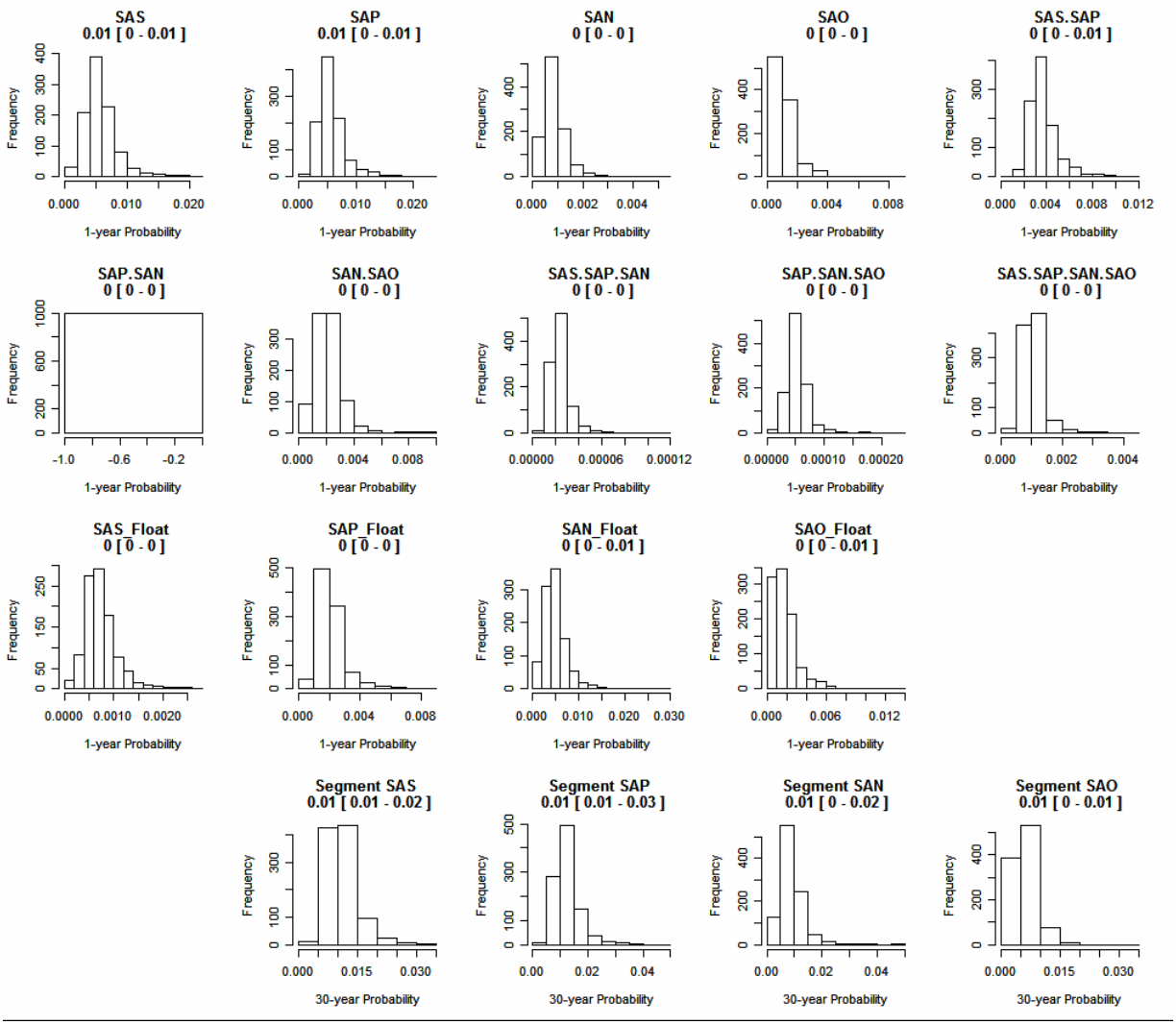

Delta Risk\Figures\TimePred2050.grf 1/31/073:45 PM

URS	DELTA RISK MANAGEMENT STRATEGY California	Time-Dependent Probabilites for the San Andreas Rupture Scenarios for 2050	Figure 6-4
	Project No. 26815621		

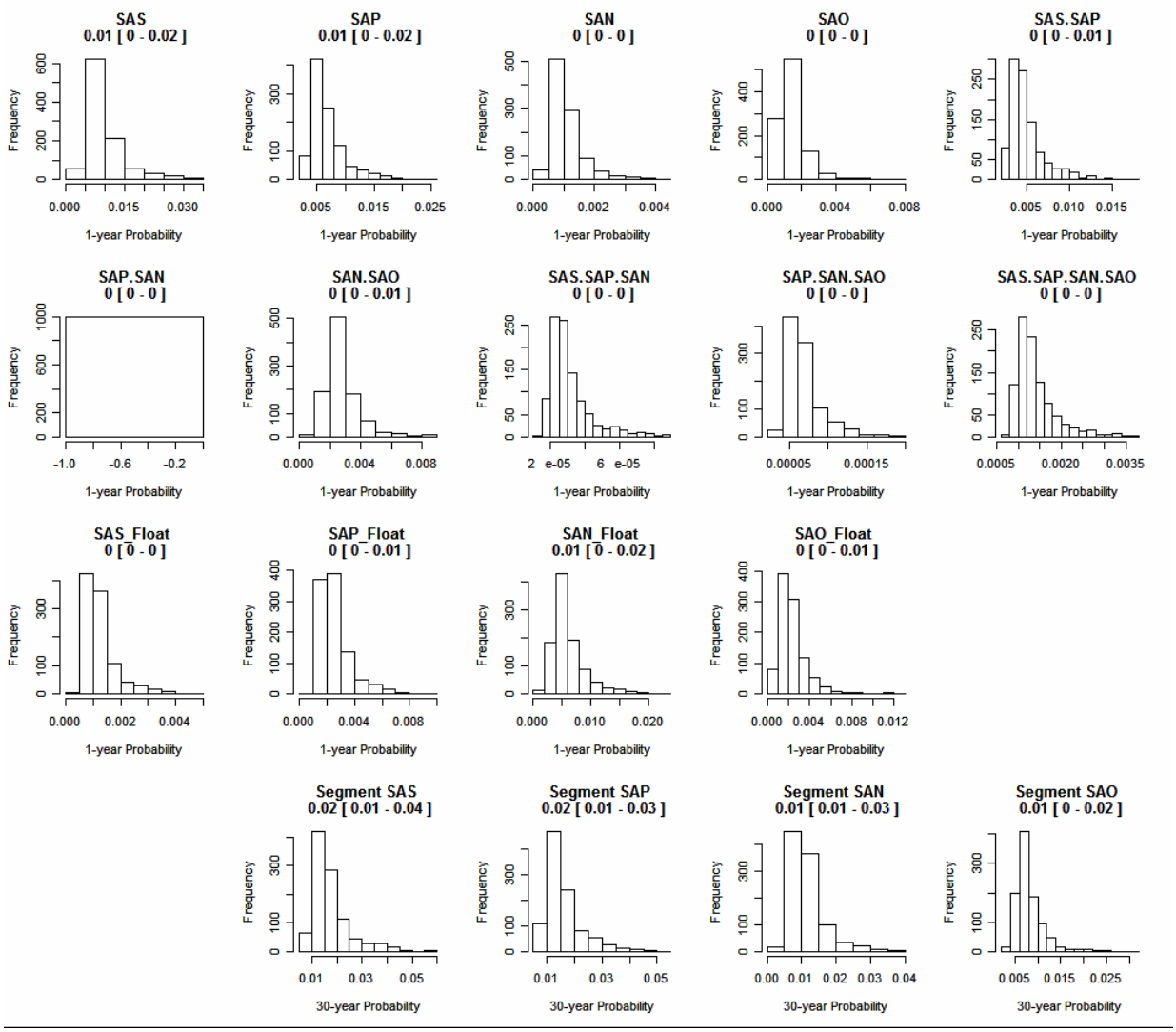

URS	DELTA RISK MANAGEMENT STRATEGY California	Time-Dependent Probabilities for the San Andreas Rupture Scenarios for 2100	Figure 6-5
	Project No. 26815621		

Delta Risk\Figures\TimePred2100.grf 1/31/073:46 PM

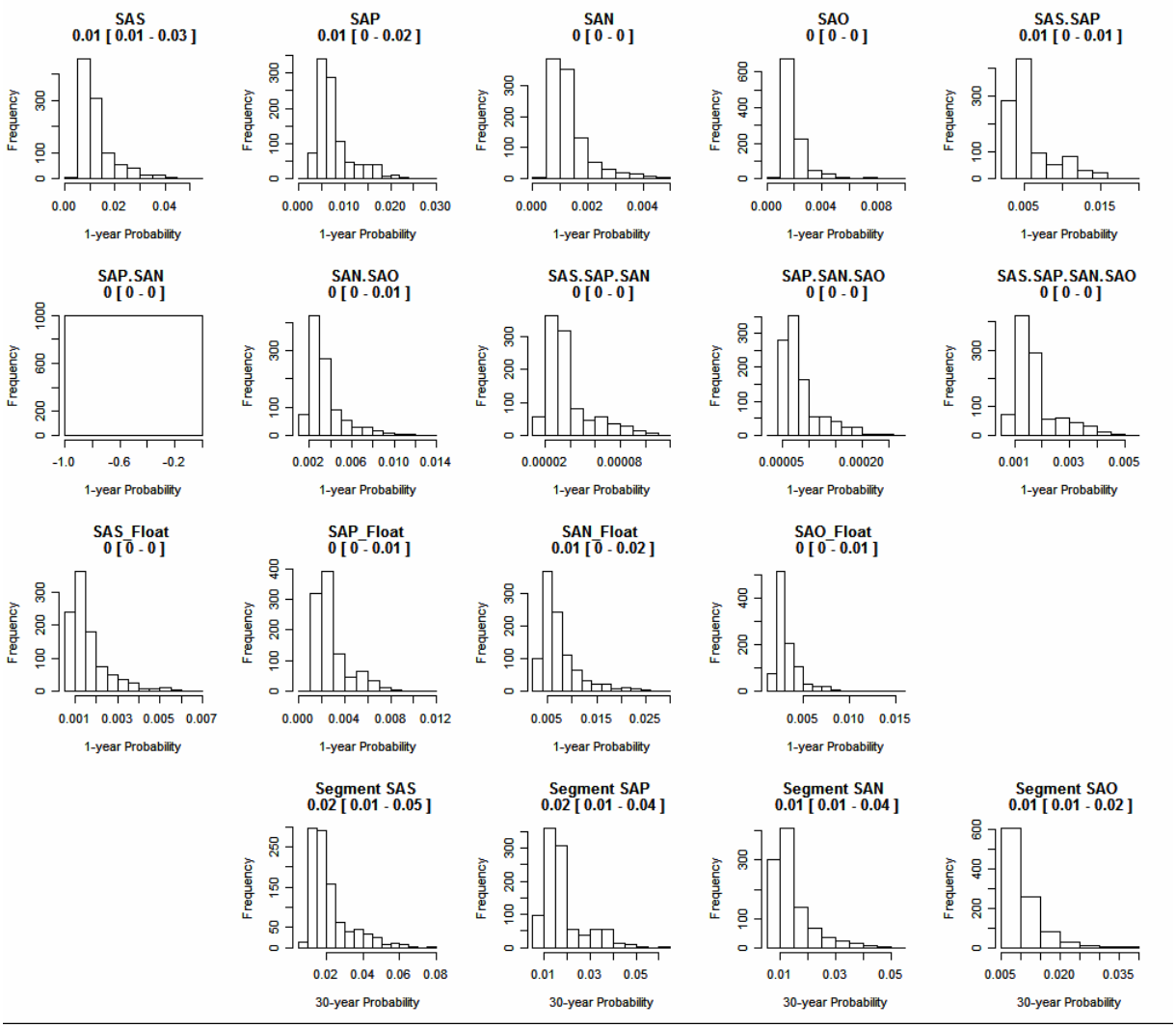

URS	DELTA RISK MANAGEMENT STRATEGY California	Time-Dependent Probabilities for the San Andreas Rupture Scenarios for 2200	Figure 6-6
	Project No. 26815621		

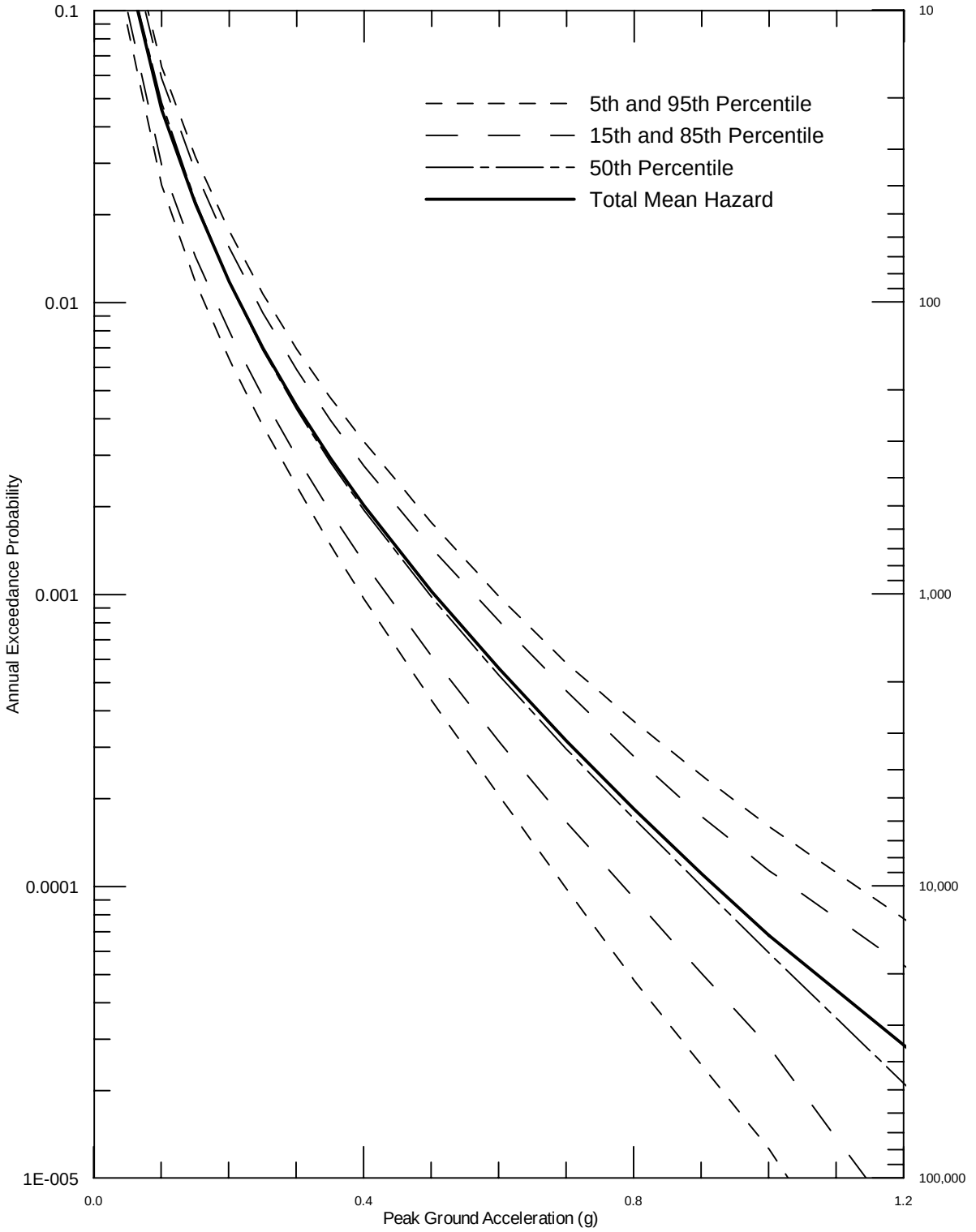

URS	DELTA RISK MANAGEMENT STRATEGY CALIFORNIA	TIME DEPENDENT SEISMIC HAZARD CURVES FOR MEAN PEAK HORIZONTAL ACCELERATION FOR CLIFTON COURT FOR 2005	Figure 6-7
	Project No. 26815900		

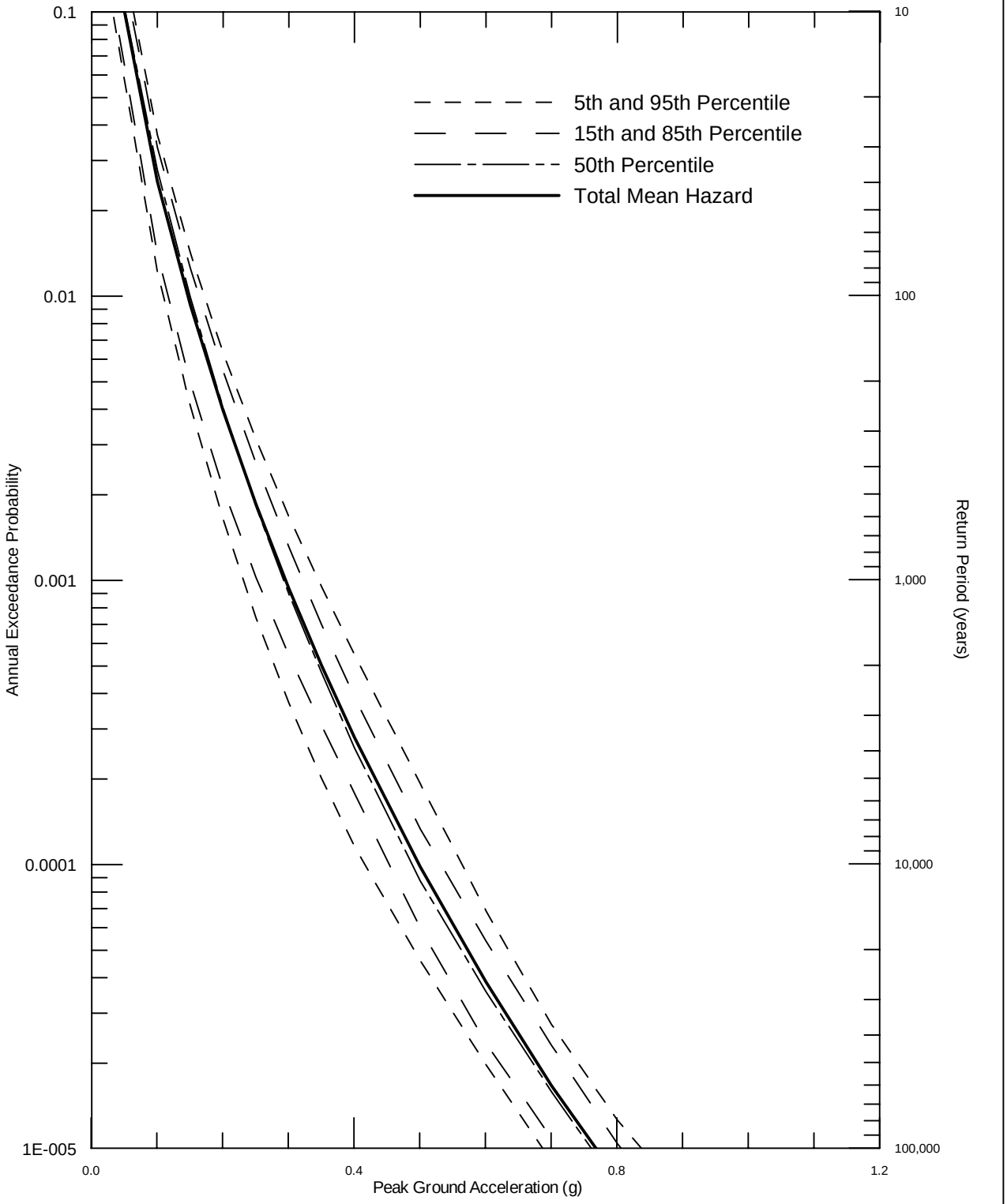

URS	DELTA RISK MANAGEMENT STRATEGY CALIFORNIA	TIME DEPENDENT SEISMIC HAZARD CURVES FOR MEAN PEAK HORIZONTAL ACCELERATION FOR DELTA CROSS CHANNEL FOR 2005	Figure 6-8
Project No. 26815900			

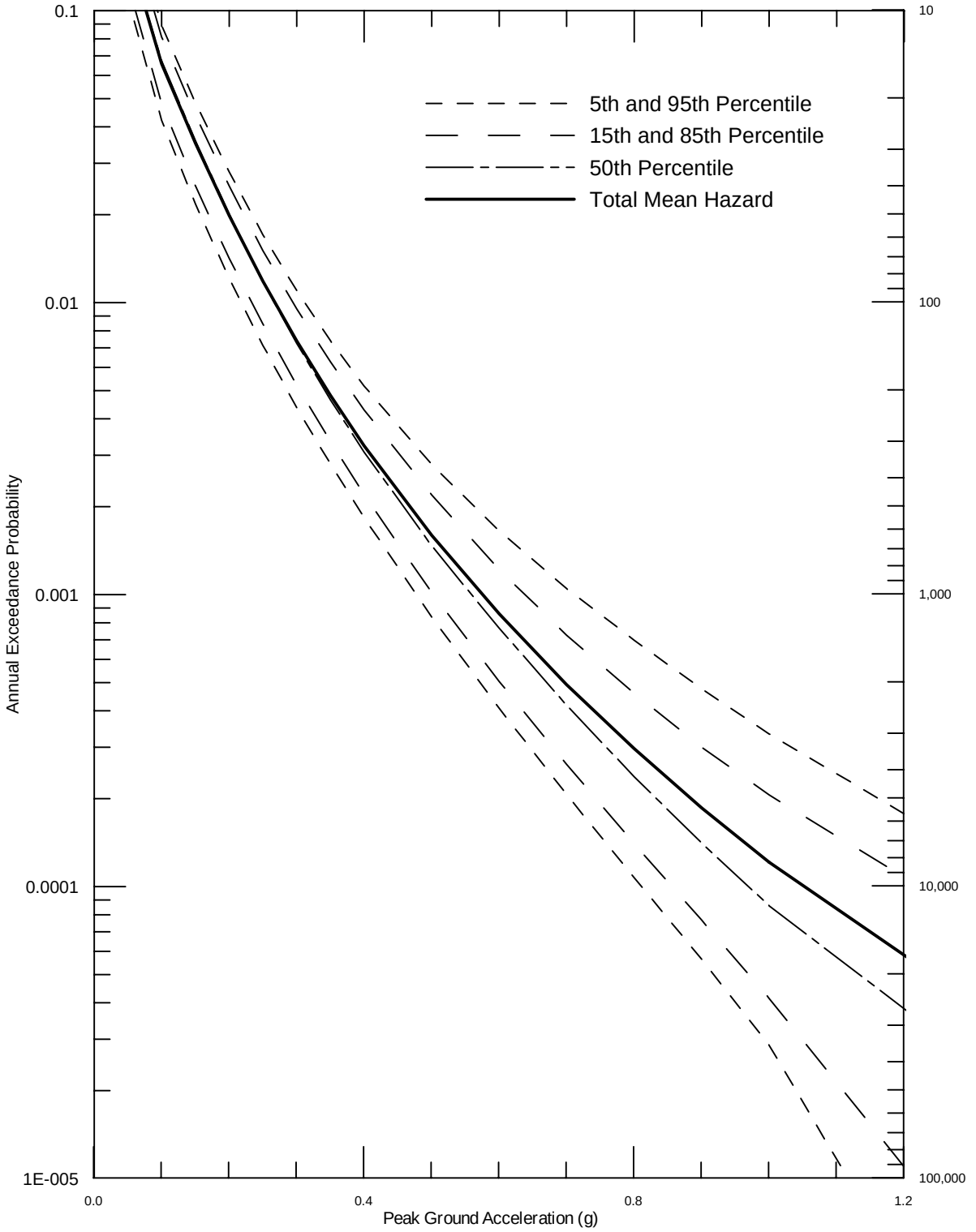

URS	DELTA RISK MANAGEMENT STRATEGY CALIFORNIA	TIME DEPENDENT SEISMIC HAZARD CURVES FOR MEAN PEAK HORIZONTAL ACCELERATION FOR MONTEZUMA SLOUGH FOR 2005	Figure 6-9
Project No. 26815900			

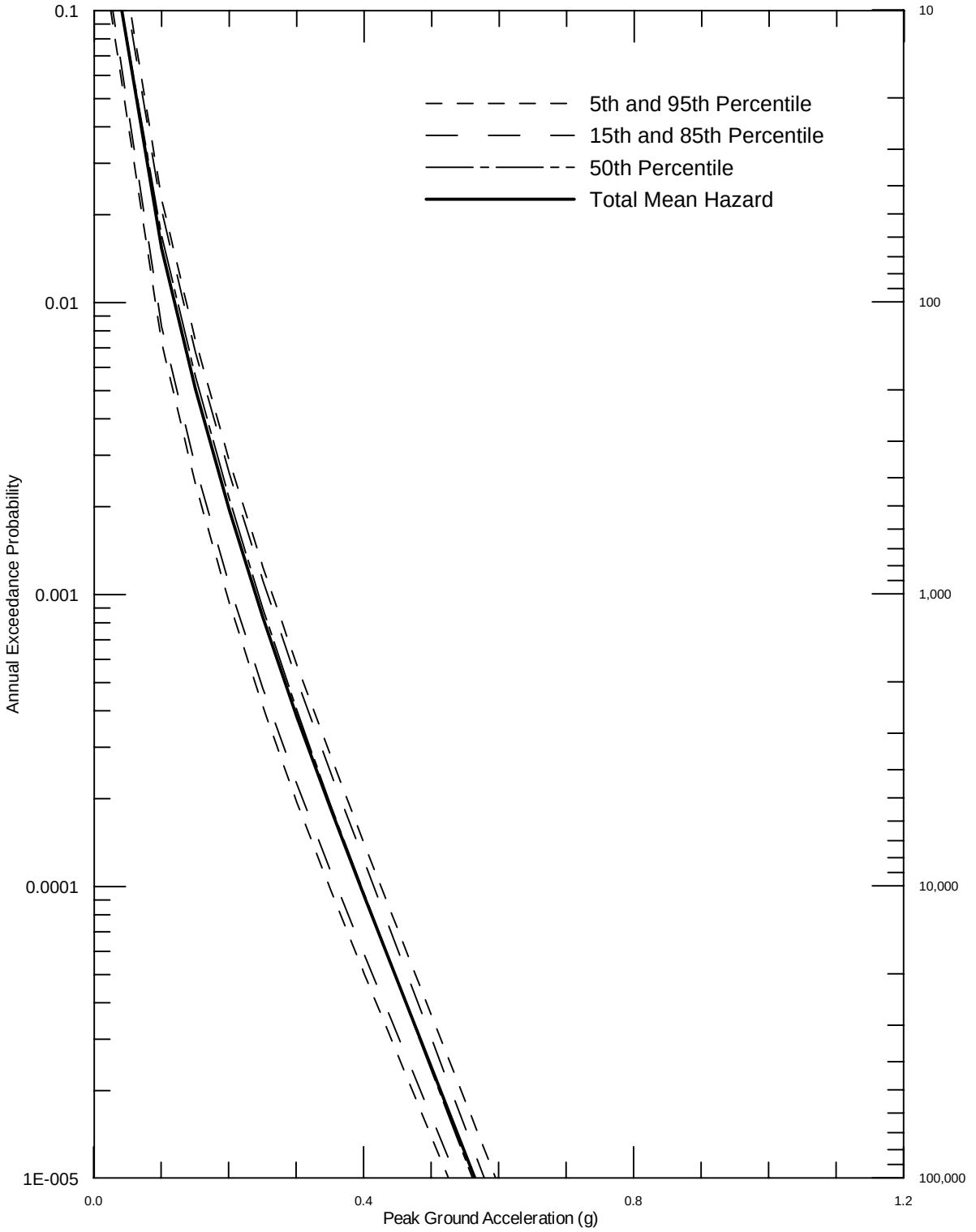

URS

DELTA RISK
MANAGEMENT STRATEGY
CALIFORNIA

Project No. 26815900

TIME DEPENDENT SEISMIC HAZARD CURVES
FOR MEAN PEAK HORIZONTAL ACCELERATION
FOR SACRAMENTO FOR 2005

Figure
6-10

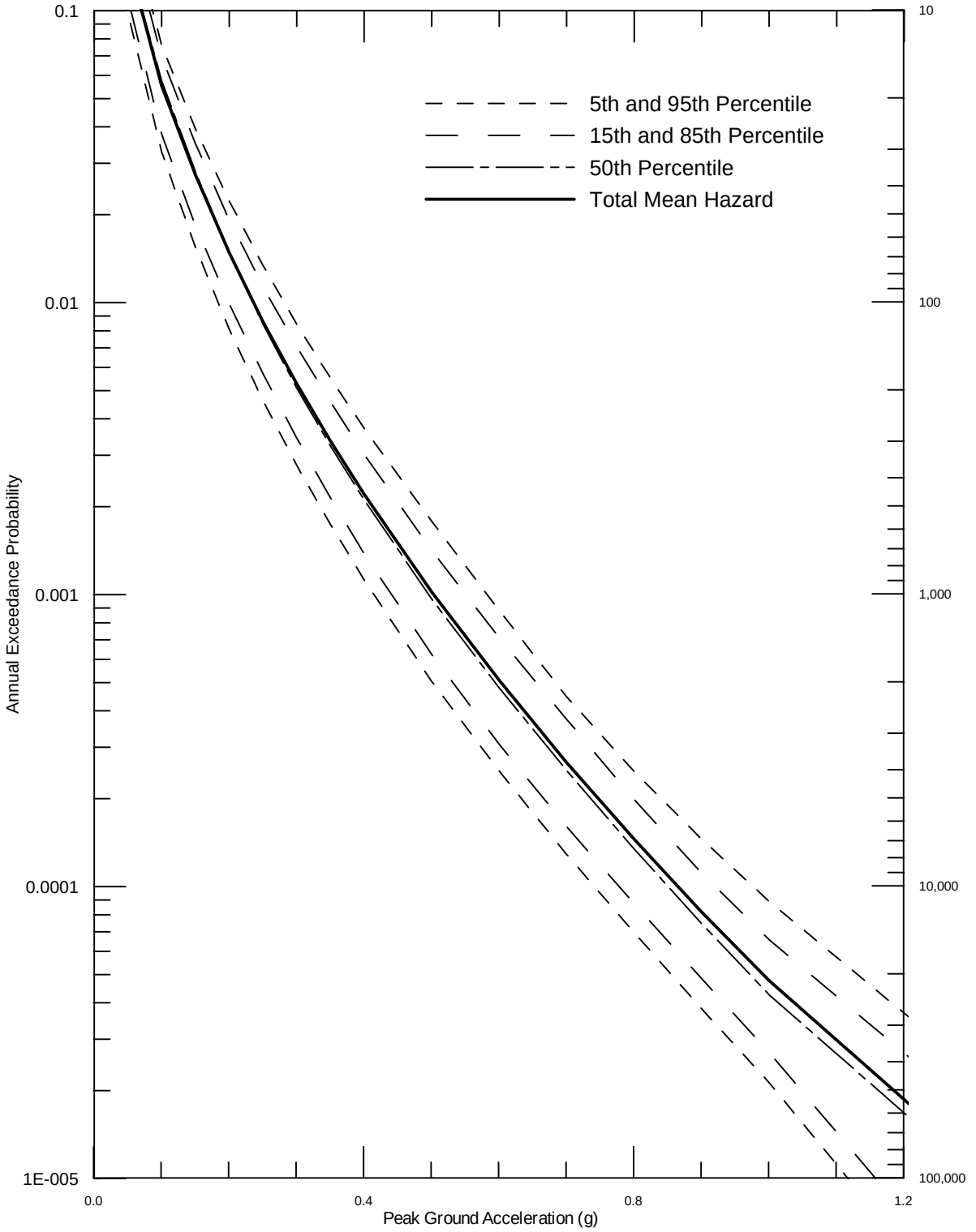

URS	DELTA RISK MANAGEMENT STRATEGY CALIFORNIA	TIME DEPENDENT SEISMIC HAZARD CURVES FOR MEAN PEAK HORIZONTAL ACCELERATION FOR SHERMAN ISLAND FOR 2005	Figure 6-11
Project No. 26815900			

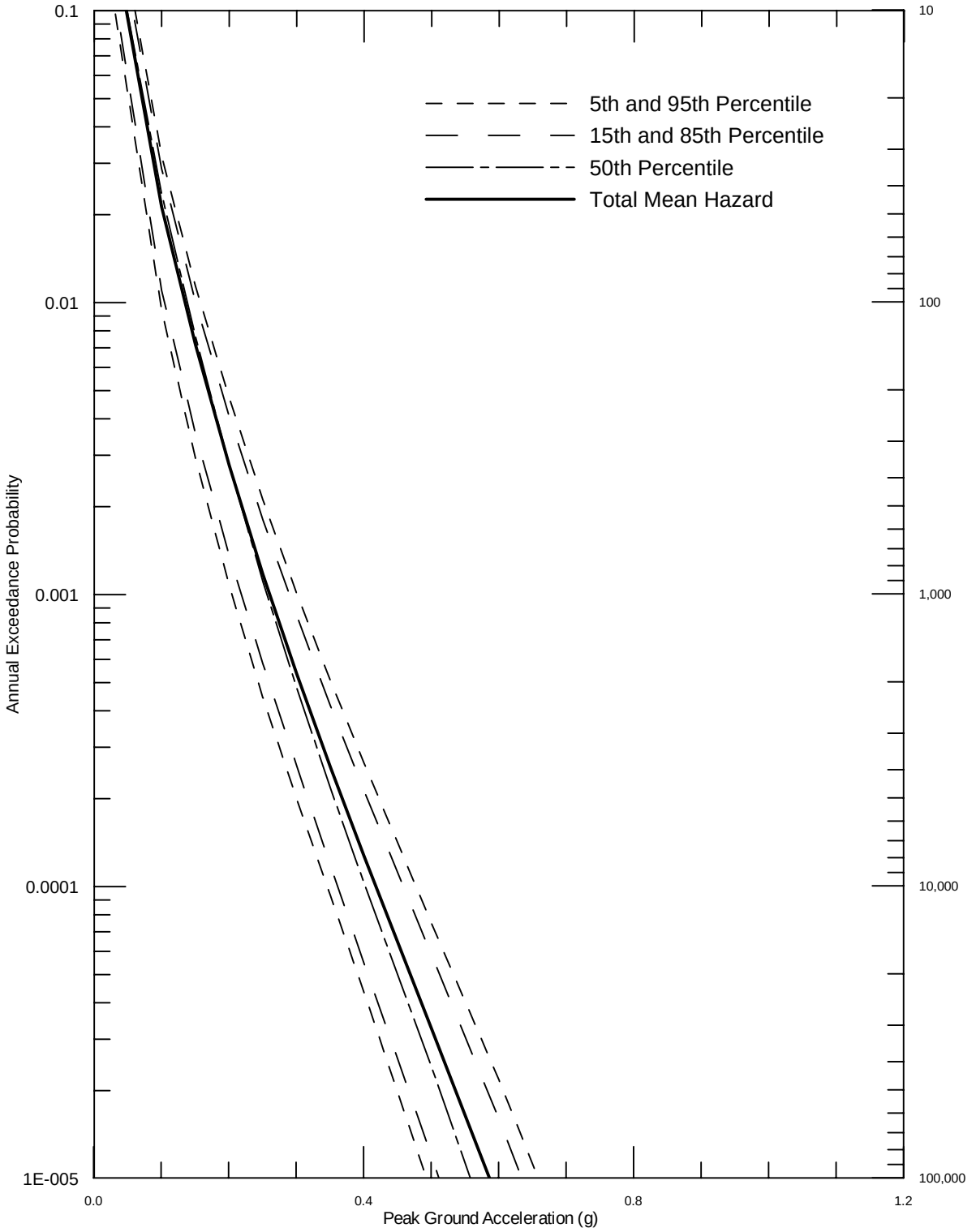

URS	DELTA RISK MANAGEMENT STRATEGY CALIFORNIA	TIME DEPENDENT SEISMIC HAZARD CURVES FOR MEAN PEAK HORIZONTAL ACCELERATION FOR STOCKTON FOR 2005	Figure 6-12
Project No. 26815900			

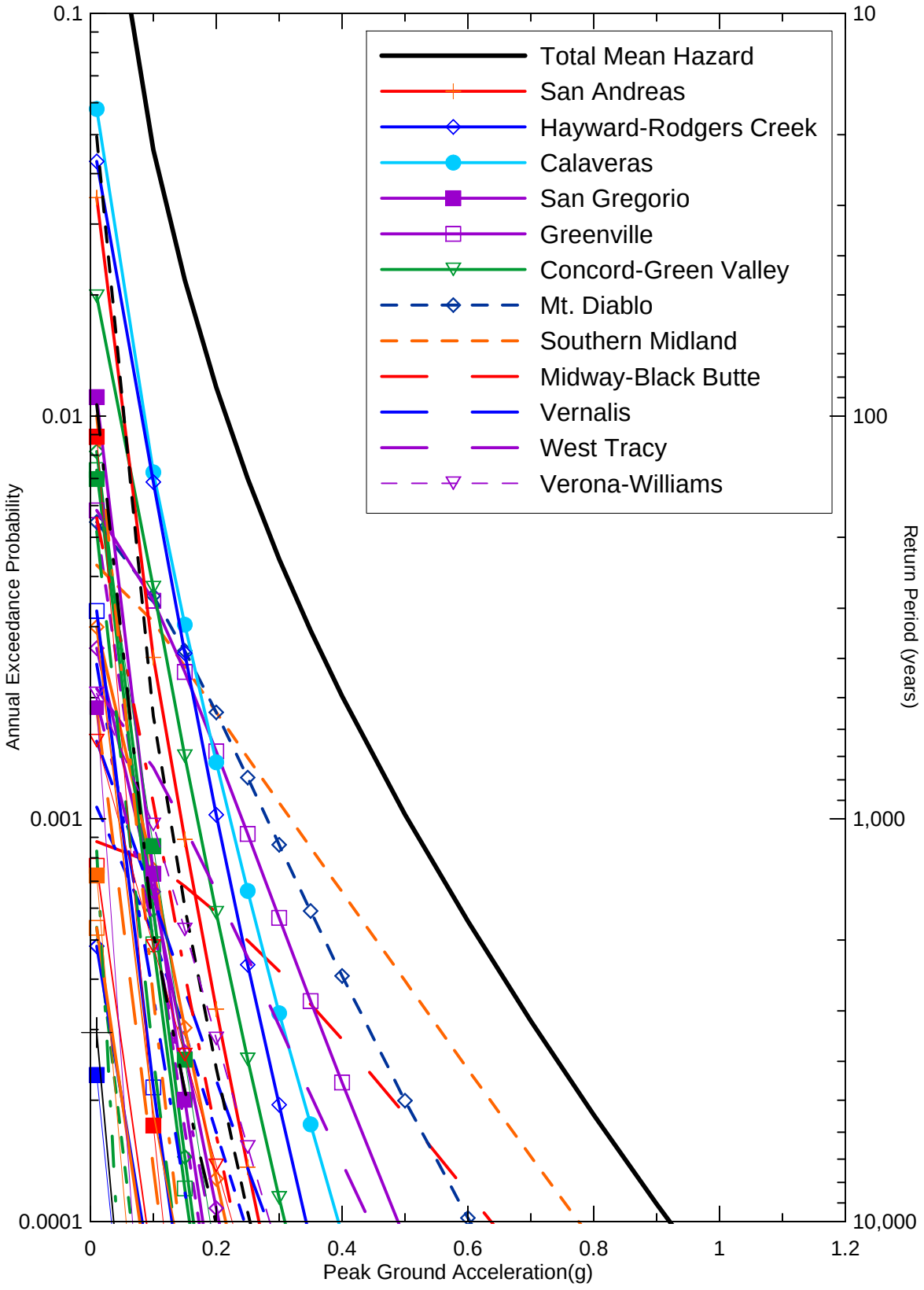

URS	DELTA RISK MANAGEMENT STRATEGY CALIFORNIA	SEISMIC SOURCE CONTRIBUTIONS TO MEAN PEAK HORIZONTAL ACCELERATION TIME-DEPENDENT HAZARD FOR CLIFTON COURT FOR 2005	Figure 6-13
Project No. 26815900			

Delta Risk\figures\DR2-pga-2005.grf

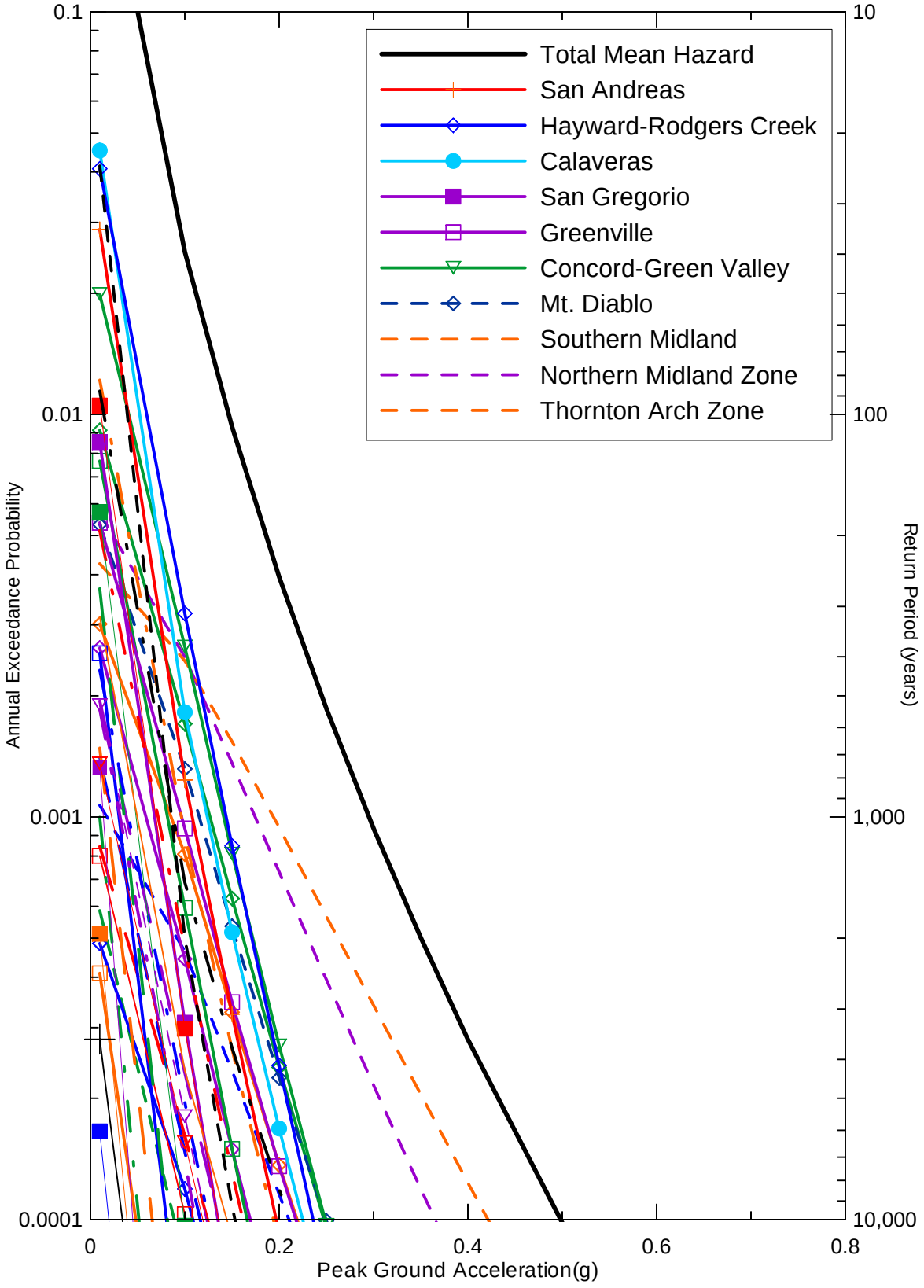

URS	DELTA RISK MANAGEMENT STRATEGY CALIFORNIA	SEISMIC SOURCE CONTRIBUTIONS TO MEAN PEAK HORIZONTAL ACCELERATION TIME-DEPENDENT HAZARD FOR DELTA CROSS CHANNEL FOR 2005	Figure 6-14
	Project No. 26815900		

Delta Risk\figures\DR4-pga-2005.grf

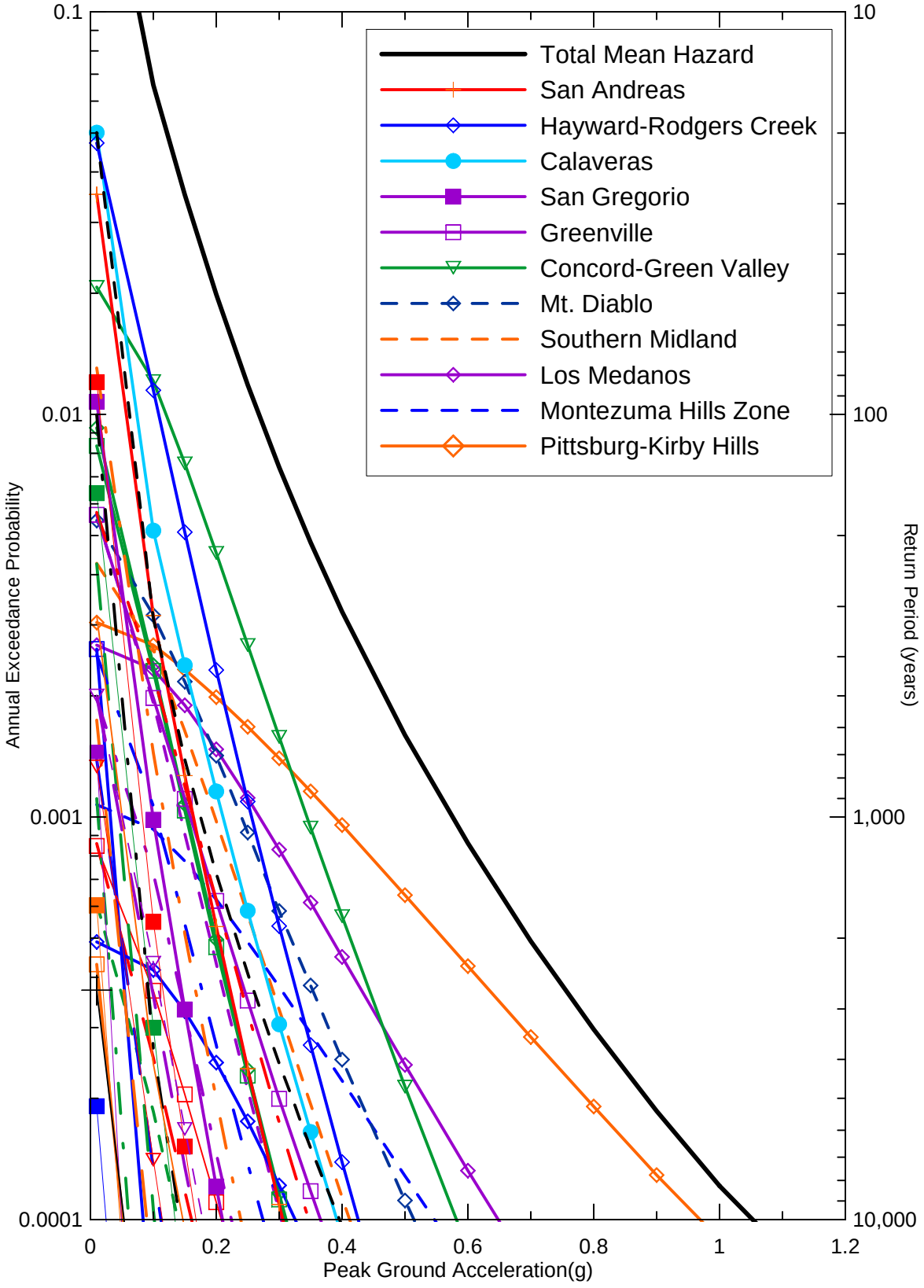

URS	DELTA RISK MANAGEMENT STRATEGY CALIFORNIA	SEISMIC SOURCE CONTRIBUTIONS TO MEAN PEAK HORIZONTAL ACCELERATION TIME-DEPENDENT HAZARD FOR MONTEZUMA SLOUGH FOR 2005	Figure 6-15
	Project No. 26815900		

Delta Risk\figures\DR3-pga-2005.grf

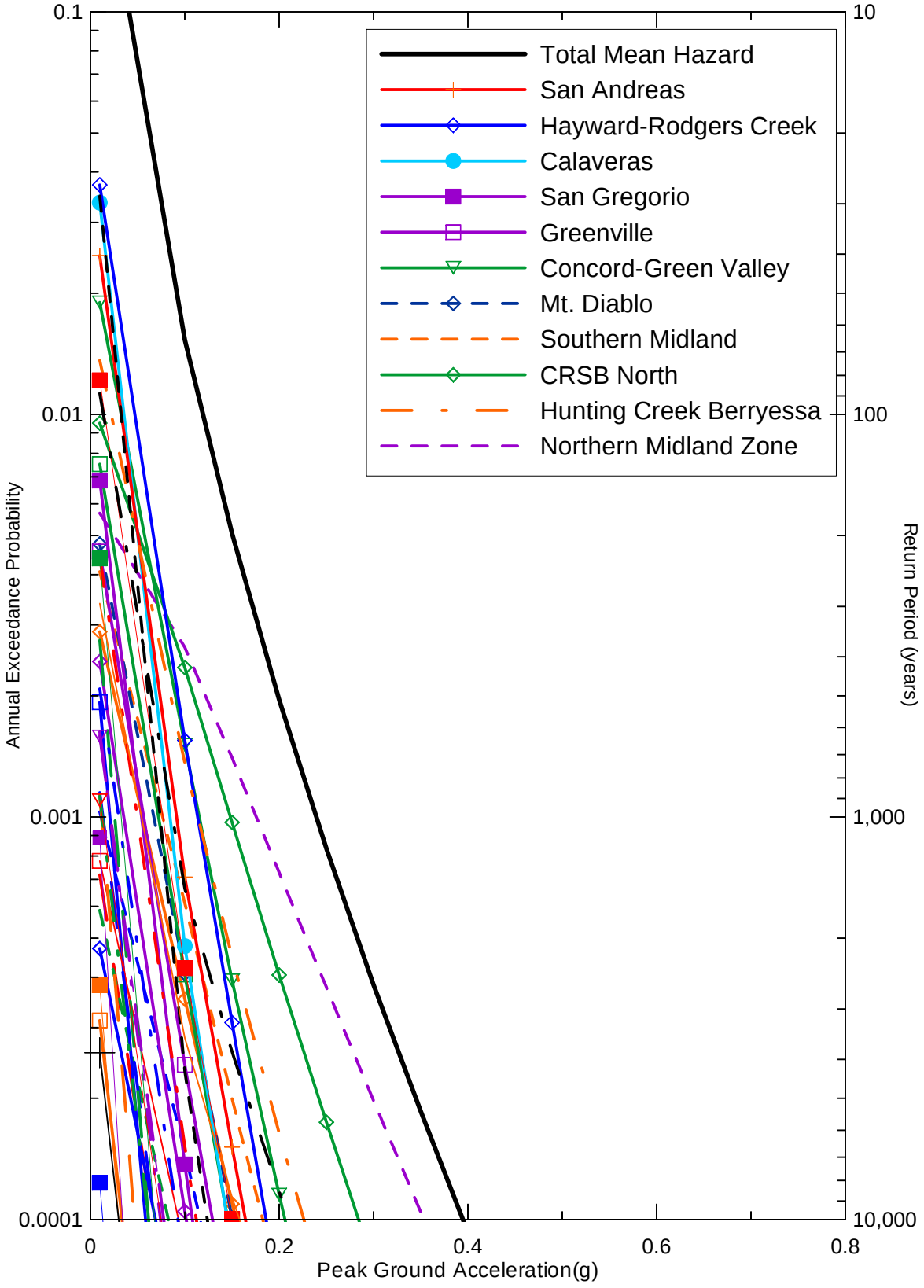

URS	DELTA RISK MANAGEMENT STRATEGY CALIFORNIA	SEISMIC SOURCE CONTRIBUTIONS TO MEAN PEAK HORIZONTAL ACCELERATION TIME-DEPENDENT HAZARD FOR SACRAMENTO FOR 2005	Figure 6-16
Project No. 26815900			

Delta Risk\figures\DR6-pga-2005.grf

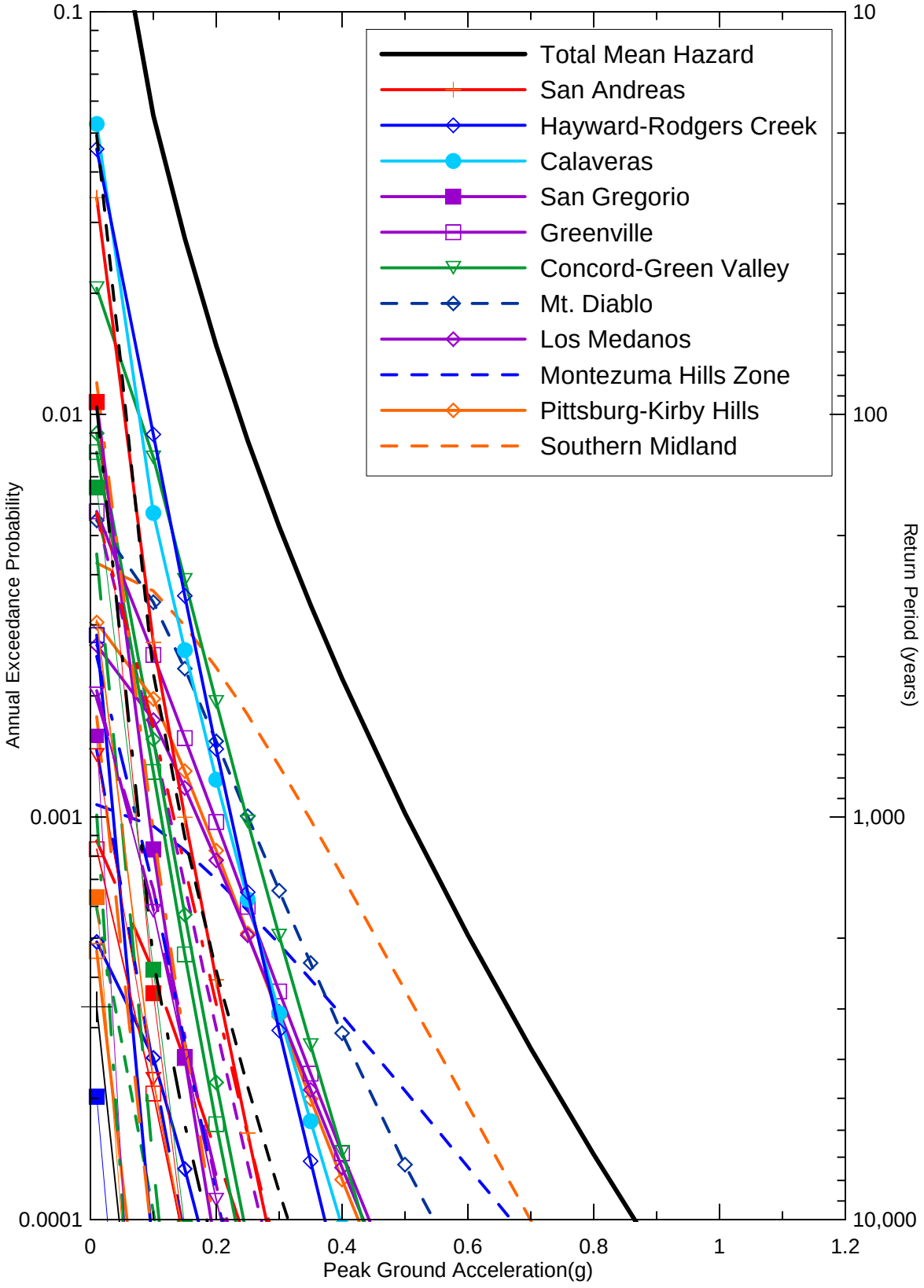

URS	DELTA RISK MANAGEMENT STRATEGY CALIFORNIA	SEISMIC SOURCE CONTRIBUTIONS TO MEAN PEAK HORIZONTAL ACCELERATION TIME-DEPENDENT HAZARD FOR SHERMAN ISLAND FOR 2005	Figure 6-17
	Project No. 26815900		

Delta Risk\figures\DR1-pga-2005.grf

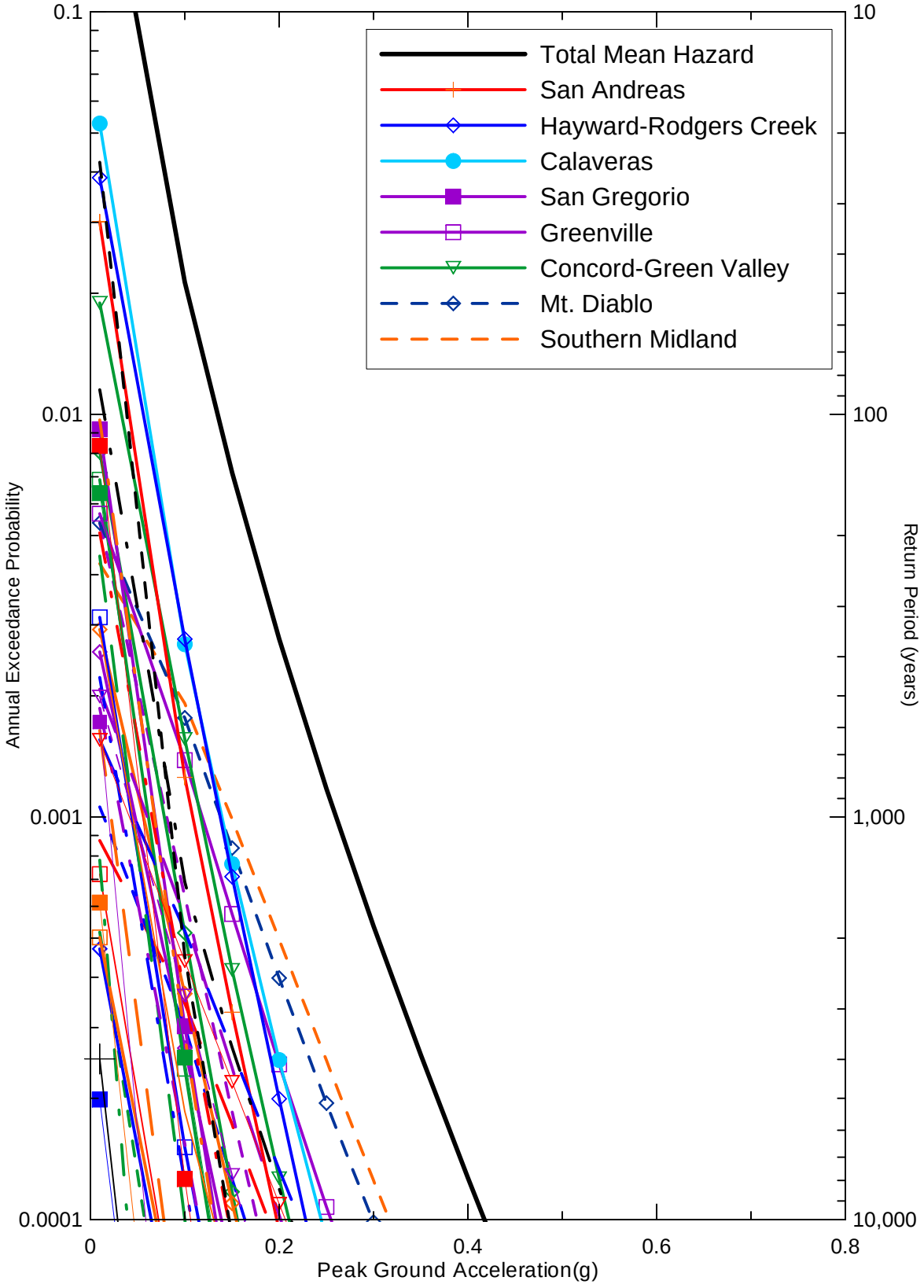

URS	DELTA RISK MANAGEMENT STRATEGY CALIFORNIA	SEISMIC SOURCE CONTRIBUTIONS TO MEAN PEAK HORIZONTAL ACCELERATION TIME-DEPENDENT HAZARD FOR STOCKTON FOR 2005	Figure 6-18
Project No. 26815900			

Delta Risk\figures\DR5-pga-2005.grf

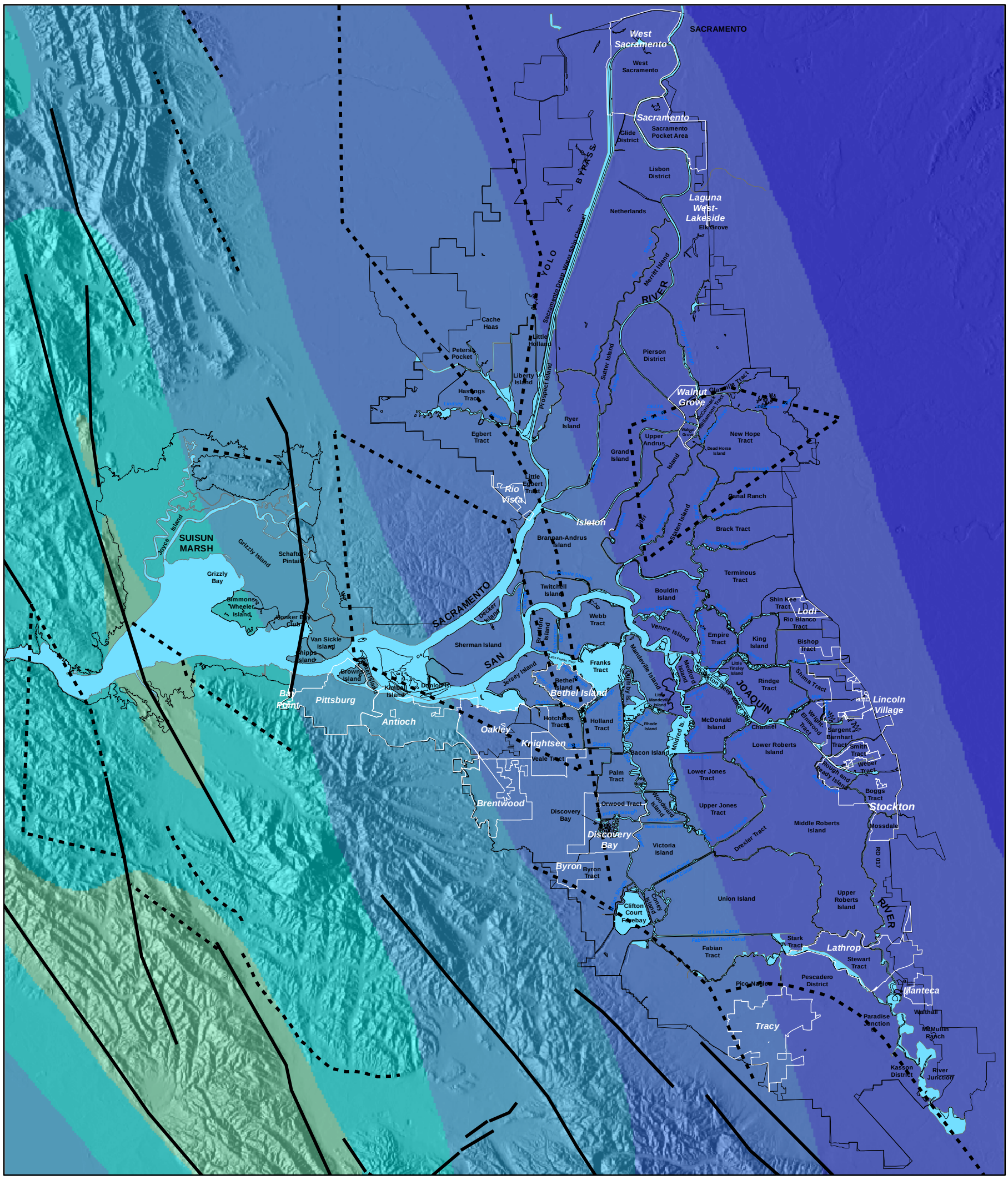

Legend

Mapped Faults

Surficial faults used in the hazard analysis

Blind Faults

Blind faults used in the hazard analysis

Legal Delta and Suisun Marsh Boundary

PGA, 100 Year Return Period

0.00 - 0.10	0.36 - 0.40
0.11 - 0.15	0.41 - 0.45
0.16 - 0.20	0.46 - 0.50
0.21 - 0.25	0.51 - 0.55
0.26 - 0.30	0.56 - 0.60
0.31 - 0.35	0.61 - 0.65
	0.66 - 0.70

0 5 10 Miles

URS

DRMS

26815431

PGA Hazard for a 100-Year Return Period

FIGURE 6-19